

***dN/dS* dynamics quantify tumour immunogenicity and predict response to immunotherapy**

**Luis Zapata^{1*}, Giulio Caravagna¹, Marc J Williams², Eszter Lakatos²,
Khalid AbdulJabbar¹, Benjamin Werner¹, Trevor A Graham^{2*}, Andrea
Sottoriva^{1*}**

¹ Centre for Evolution and Cancer, Institute of Cancer Research, London, UK

² Centre for Genomics and Computational Biology, Barts Cancer Institute, Barts and the London School of Medicine and Dentistry, Queen Mary University of London, UK

* Correspondence to: luis.zapata@icr.ac.uk, t.graham@qmul.ac.uk and andrea.sottoriva@icr.ac.uk

Abstract

*Immunoediting is a major force during cancer evolution that selects for clones with low immunogenicity (adaptation), or clones with mechanisms of immune evasion (escape). However, quantifying immunogenicity in the cancer genome and how the tumour-immune coevolutionary dynamics impact patient outcomes remain unexplored. Here we show that the ratio of nonsynonymous to synonymous mutations (*dN/dS*) in the immunopeptidome quantifies tumor immunogenicity and differentiates between adaptation and escape. We analysed 8,543 primary tumors from TCGA and validated immune *dN/dS* as a measure of selection associated with immune infiltration in immune-adapted tumours. In a cohort of 308 metastatic patients that received immunotherapy, pre-treatment lesions in non-responders showed increased immune selection ($dN/dS < 1$), whereas responders did not and instead harboured a higher proportion of genetic escape mechanisms. Ultimately, these findings highlight the potential of evolutionary genomic measures to predict clinical response to immunotherapy.*

34 Introduction

35

36 Cancer is an evolutionary process, where natural selection acts upon somatic
37 mutations that alter phenotypes, and drives adaptation^{1,2}. Recent advances in
38 genomic technologies have enabled the characterisation of mutational
39 landscapes in thousands of malignant^{3,4}, and healthy somatic tissues^{5,6,7,8}. These
40 studies found that a) 2 to 5 driver mutations are sufficient to initiate a malignancy,
41 b) driver mutations are also present in normal tissue^{5,6,7}, c) 90-95%% of somatic
42 point mutations are neutral⁷⁻⁹, and d) the signals of negative selection in somatic
43 tissues are weaker compared to germline evolution^{7,10}. However, the roles of
44 negative, positive, and neutral evolution during carcinogenesis remains
45 debated¹¹, especially with regards to the extent of neutral evolution¹²⁻¹⁴ and
46 negative selection^{7,8,15,16}.

47

48 The application of evolutionary theory allows us to infer cell growth dynamics, the
49 number of driver alterations^{17,18} and their selective fitness coefficients¹⁹⁻²², as well
50 as the impact of deleterious mutations during cancer progression^{23,24}. An
51 evolutionary metric recently used to detect selection in cancer studies is the ratio
52 of nonsynonymous to synonymous mutations, dN/dS ^{7,8,25-27}. The rationale is that
53 within a genomic locus, nonsynonymous mutations that decrease cell fitness will
54 show a paucity (negative selection, $dN/dS < 1$) while nonsynonymous mutations
55 that increase cell fitness will be more frequent (positive selection, $dN/dS > 1$)
56 compared to synonymous neutral mutations. Mutations modulate fitness by
57 altering the birth-death rate of a cell (driver and deleterious mutations) or by
58 causing immune-mediated predation of the lineage (neoantigens or immunogenic
59 mutations). We recently explored the evolutionary dynamics caused by negative
60 selection operating in cancer, demonstrating that negative selection – and its
61 release by immune escape – leads to a predictable neoantigen variant allele
62 frequency (VAF) distribution²⁸. In theory, the shape of the neoantigen VAF
63 distribution can measure selection, but technical limitations around neoantigen
64 detectability in standard genome sequencing make the method impractical and
65 under-powered. Here we show how dN/dS -based measures offer a robust

66 means to quantify negative selection strength and detect competing selective
67 forces acting in distinct regions of the cancer genome.

68

69 The notion that the immune system influences cancer progression originated in
70 the early 1900s^{29,30}. It was only a century later, that studies in mice demonstrated
71 that genetically inbred mice lacking lymphocytes, developed more spontaneous
72 and chemically induced tumors than their wild-type counterparts^{30–32}. These
73 results engendered the concept of cancer immunoediting where tumor cells are
74 subject to three phases: elimination, equilibrium, and escape²⁹. Cancer
75 immunoediting is an evolutionary process that shapes tumour immunogenicity by
76 selecting for clones depleted of neoantigens (immune-adapted) or with an
77 immune evasion phenotype (immune-escaped)^{33–35}. Neoantigens are generated,
78 among other mechanisms, by single nucleotide variants (SNVs) leading to
79 aminoacidic changes in a peptide previously recognized as a self-antigen³⁶.
80 However, the extent of immunogenicity derived from SNVs in self-antigens
81 remains unclear, particularly if anchor positions of the wild-type peptide are
82 affected³⁷. In our previous work, we observed signals of immune-mediated
83 negative selection in the immunopeptidome, defined as all natively MHC-bound
84 genomic regions, associated to levels of immune infiltration. Nonetheless, a
85 recent study claimed that after applying a more stringent normalization method
86 these regions do not harbour signals of selection¹⁶. In this work, we corroborated
87 our earlier findings and we further provide an alternative explanation for the lack
88 of signal reported recently.

89

90 The recent discovery of immune checkpoints (e.g. PD1 or CTLA4) as mechanism
91 of immune evasion, led to the development of cancer therapies using immune
92 checkpoint inhibitors (ICIs). Despite the promising clinical results of ICIs, only
93 30% of patients treated with these therapies show significant response.
94 Therefore, considerable effort has been dedicated to understand the interaction
95 between the immune system and cancer^{38–43}, and to identify genetic
96 determinants of immunotherapeutic response. To date, quantification of tumor
97 mutation burden (TMB) is the primary genomic biomarker for enrolling patients

98 into ICI treatment. The underlying hypothesis for TMB as a biomarker is that a
99 higher number of somatic mutations leads to a higher number of neoantigens,
100 and therefore a higher likelihood of immune clearance after checkpoint inhibition.
101 However, recent studies have shown that even mismatch repair proficient tumors
102 display a pathological response⁴⁴, emphasizing the need for quantifying the true
103 immunogenicity of the cancer genome and their potential clinical response to
104 immunotherapy.

105

106 Here, we modelled cancer initiation and progression by adapting a stochastic
107 branching process⁴⁵ to simulate changes in dN/dS over time as a measure of
108 selection and tumor immunogenicity during immunoediting. Using the insight
109 gained from our model, we assessed dN/dS values in 8543 primary tumours, as
110 well as 308 metastatic cancers treated with ICIs. We first corroborate that immune
111 dN/dS correlates with levels of tumor infiltrating lymphocytes – a measure of the
112 strength of immunoediting - in non-escaped tumors. Finally, by estimating
113 immune dN/dS in pre-treated patients, we reported clinical response in immune-
114 escaped patients that had an absence of immune selection (immune $dN/dS \sim 1$).
115 In contrast, tumors with low immune dN/dS , and therefore low levels of tumor
116 immunogenicity, did not respond to the action of immune checkpoint inhibitors.

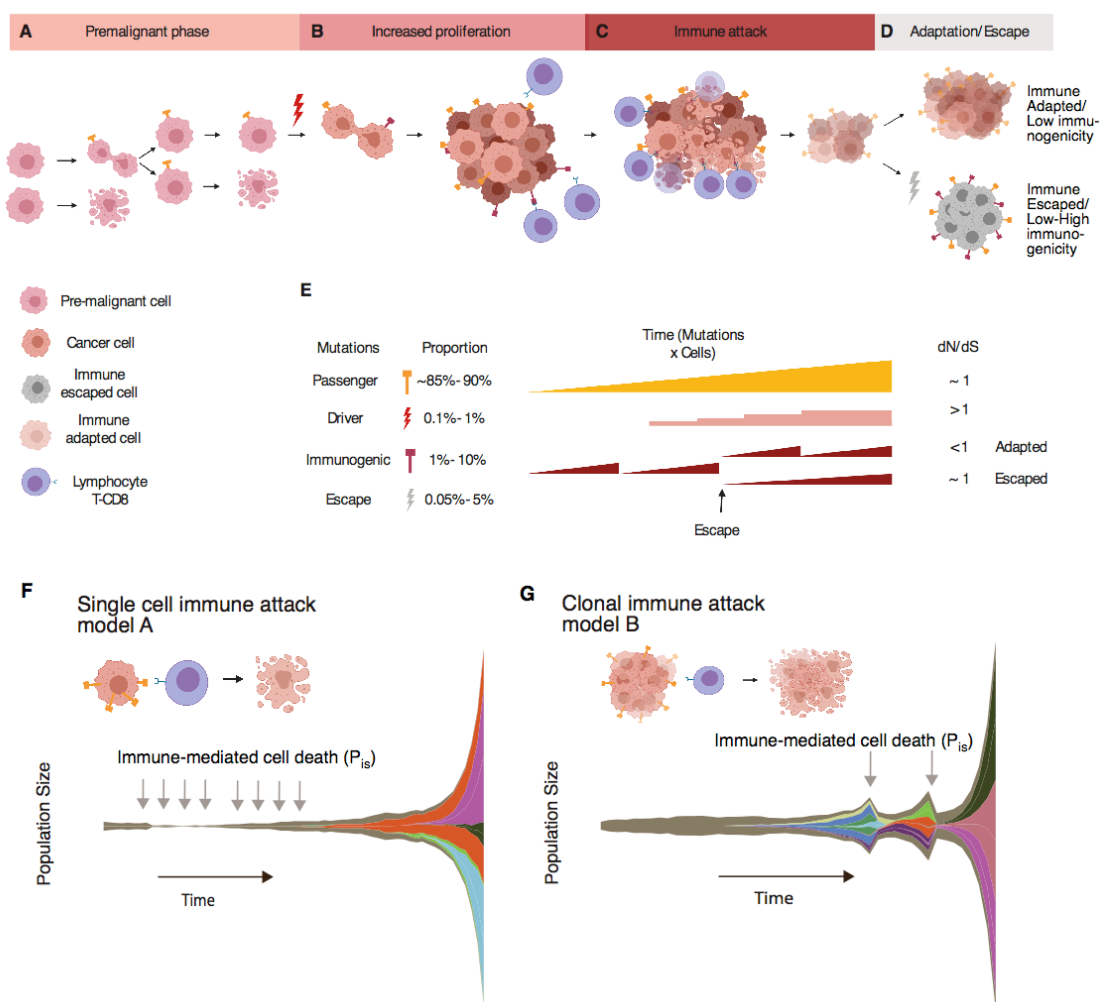
117

118 **Results**

119 **A mathematical model of immunoediting**

120 We extended our previous modelling work to incorporate the acquisition of
121 nonsynonymous and synonymous mutations in driver (positively selected) and
122 passenger (neutral) loci^{24,46,47}, as well as in regions exposed to the immune
123 system and regions that confer immune-evasion properties (Fig 1). The
124 interaction of different mutations and the observed evolutionary dynamics can be
125 simplified into four phases: 1) A pre-neoplastic phase where cells do not have
126 cancer driver mutations but may acquire passenger, immunogenic or escape
127 mutations (Fig 1A), 2) a neoplastic phase that begins when a driver mutation
128 avoids stochastic drift and initiate a clonal expansion (Fig 1B), 3) an elimination
129 phase where cells acquiring somatic mutations recognized by the immune

130 system are eliminated (Fig 1C), and 4) a phase where expanding clones lead to
 131 a clinically-detectable tumor through either depletion of immunogenic mutations
 132 (immune adapted) or through a mutation in the genome that triggers an immune
 133 escape mechanism (immune escaped) (Fig 1D). An activated escape mechanism
 134 hides the clone from the immune system so that neoantigens accrue without
 135 being depleted by negative selection raising the overall tumor immunogenicity
 136 (Fig S1A). It is possible for these phases to overlap each other. For example, an
 137 escape mutation occurring pre-driver acquisition and thus pre-clonal expansion
 138 leads to tumors "born" immune-escaped.
 139



140

141 *Figure 1. Description of the stochastic branching process used to model immunoediting. A) An initial set of*
 142 *wild type cells (Pre-malignant cell) divide and accumulates mutations. B) A driver mutation increases the*
 143 *probability of cell division initiating a phase of increased proliferation of clones (Cancer cell). C) During the*
 144 *phase of immune attack, the immune system removes cells carrying immunogenic mutations and might*
 145 *eradicate the tumor completely or force the tumor to adapt or escape. D) Two possible scenarios emerge*
 146 *as the outcome of immunoediting, cancer cells survive not harbouring immunogenic mutations (Immune*
 147 *adapted) or due to the acquisition of an immune evasion mechanism (Immune escaped). E) These scenarios*

148 *can be differentiated by looking at the ratio of nonsynonymous to synonymous mutations (dN/dS) in immune*
149 *exposed regions of the genome. We defined two hypotheses of immune recognition: F) Single cell immune*
150 *attack where any single cell carrying a neoantigen is able to initiate an immune response and be eliminated*
151 *at a rate of immune-mediated cell death of P_{IS} , G) Clonal immune attack where a minimum percentage of*
152 *immunogenic cells is needed to elicit an immune response, as recently observed in mice models⁴⁸.*

153
154 We initiated our model in the pre-neoplastic phase with a pool of N cells having
155 an equal probability of birth (b) and death (d): $b=d=0.5$ (Methods). For each
156 successful cell division, a number of new mutations are sampled from a Poisson
157 distribution with mean $\mu \times L$ (mutation rate measured in mutations per base pair
158 per cell division multiplied by the length of the coding genome, L). We introduced
159 nonsynonymous and synonymous mutations at a constant relative rate of 3 to 1
160 given the expected genome composition⁴⁹, so we could calculate the ratio
161 between these two types of mutations (dN/dS) in the evolved population of
162 tumour cells. We assumed that passenger nonsynonymous and all synonymous
163 mutations are neutral. Once a cell acquired a nonsynonymous mutation in a
164 driver, the probability of cell division b increases by a fixed value obtained from a
165 Gompertz function (Methods), driving the next stage of tumorigenesis.

166
167 During immunoediting^{29,50}, cells carrying an immunogenic mutations may elicit an
168 immune response. We tested whether or not dN/dS values derived from the
169 immunopeptidome, the portion of the genome constantly exposed to immune
170 recognition (defined as 'Immune dN/dS '), quantifies overall tumor
171 immunogenicity, and differentiates between adaptation and escape. We
172 expected that when the immune predation was active and there were no escape
173 mechanisms evolved, the immune dN/dS would be lower than 1 showing overall
174 low tumor immunogenicity. Conversely, in the presence of escape mechanisms
175 immune dN/dS would have values closer to 1, and therefore high
176 immunogenicity. Additionally, we could also measure a 'global dN/dS ' by using
177 mutations in all loci of the genome, and a 'driver dN/dS ' by considering only
178 mutations in driver loci (Fig 1E). We then modelled two hypotheses of immune
179 recognition (Fig S1B): (1) a classic model (model A) where a single cell carrying
180 an immunogenic mutation is sufficient to elicit an immune response (Fig. 1F), and
181 (2) a clonal model (model B), recently suggested⁴⁸, where a percentage

182 *Pclonesize* of the total cells carrying the same immunogenic mutation is needed
183 for the immune system to attack (Fig. 1G). In model A, the immune system is
184 constantly pruning immunogenic cells, whereas model B produces a "rise and
185 fall" pattern where immunogenic cells are allowed to expand to a threshold size
186 but are then eliminated, similar to mass extinction events. Cells bearing a
187 neoantigen are killed at an immune-mediated cell death rate P_{IS} , where $P_{IS} \in$
188 $[0,1]$. This parameter models the stochastic probability of encounters between
189 antigen presenting cells and cytotoxic T-cells. Model parameters are summarized
190 in Supplementary Table 1.

191

192 **Evolutionary dynamics of dN/dS during immunoediting reveals genomic** 193 **signals of tumor immunogenicity**

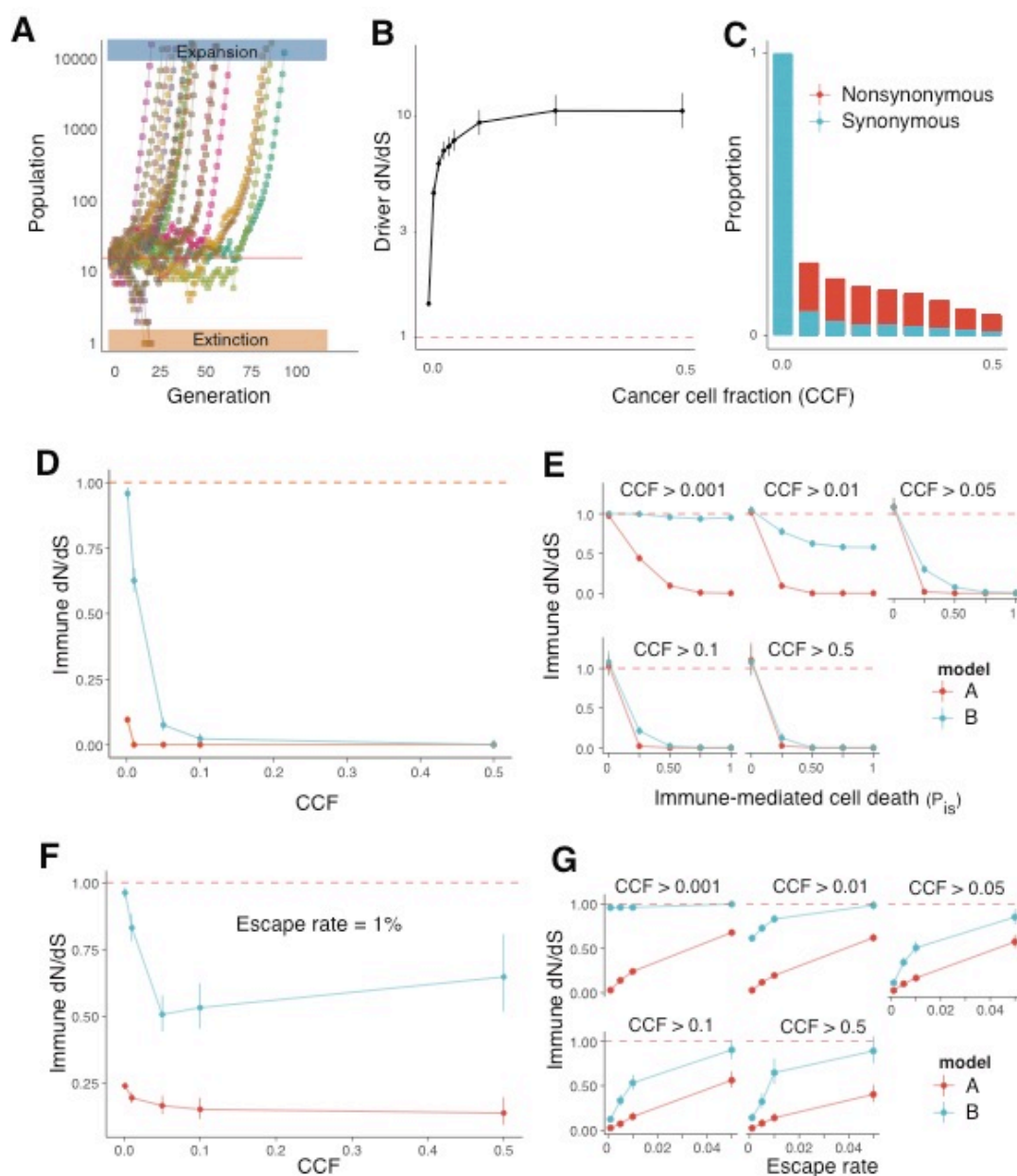
194

195 To first understand dN/dS dynamics during the pre-neoplastic phase, we
196 simulated the acquisition of neutral mutations only (non-synonymous passenger
197 and synonymous mutations) in an initial population of 32 cells for 30 generations
198 (Fig S2). We compared three mutation rate regimes similar to those found in
199 some neoplasms: microsatellite stable ($\mu\text{MSS}=10^{-8}$ mutations/bp/division),
200 microsatellite unstable ($\mu\text{MSI}=10^{-7}$), and POLE-like ($\text{POLE}=10^{-6}$). On average,
201 the population size remained constant over time for the three regimes and the
202 number of mutations was higher for higher mutation rate regimes (Fig S2A-B).
203 The average number of mutations per simulated population was 10^2 , 10^3 , and 10^4
204 for each mutation rate regime respectively (Fig S2B). As expected under neutral
205 dynamics, we observed that the average dN/dS did not deviate significantly from
206 1 and the variance was lower at high mutation rates. (95%CI for 10^{-8} : 0.54-2.31,
207 MSI:0.79-1.30, POLE:0.91-1.06) (Fig S2C).

208

209 To determine the influence of positive selection on dN/dS values over time during
210 the increased proliferation phase, we simulated only passenger and driver
211 events. We simulated 1000 datasets assuming 0.1%, 0.5% and 1% of driver sites
212 (Fig S3). We focused our analysis on simulations where a clonal expansion
213 occurred, as defined by a growing population of more than 1000 cells within 100

214 generations (Fig 2A). We calculated dN/dS over time for all mutations (global
215 dN/dS) and for only driver mutations (driver dN/dS). We observed large
216 fluctuations of the global dN/dS values among the first generations due to the low
217 number of mutations (Fig S3D). Interestingly, the accumulation of neutral variants
218 pushed global dN/dS values to 1. Driver dN/dS peaked at high values and
219 subsequently decreased towards one due to the accumulation of low frequency
220 neutral variants (Fig S3E). As we demonstrated in Williams et al²¹, mutation
221 frequency and driver dN/dS are expected to be positively associated showing the
222 highest values at the largest clone sizes (Fig 2B). Accordingly, and as observed
223 recently in clonal hematopoiesis²², the allele frequency spectrum (Cancer Cell
224 fraction or CCF) of synonymous and non-synonymous mutations (Fig. 2C)
225 showed that the observed high driver dN/dS is a consequence of proportionally
226 fewer synonymous mutations at higher CCF thresholds compared to
227 nonsynonymous mutations.



228

229 *Figure 2. Immunoediting leads to tumor adaptation or escape. A) We defined two outcomes for each*
 230 *simulation: expansion and extinction. Expansion: Clonally expanded populations (Blue) that reached an*
 231 *upper limit of number of cells in the first n generations. Extinction: Simulations that drifted to extinction*
 232 *among the first n generations (Orange). B) driver dN/dS relationship to the cancer cell fraction. As described in*
 233 *Williams et al²¹ we show in our model that driver dN/dS increases at increasing values of clonality. C)*
 234 *Relative proportion of nonsynonymous to synonymous mutations. The upward trend of dN/dS is due to a*
 235 *high proportion of synonymous mutations removed at increasing CCF cut-offs. D) Immune dN/dS*
 236 *relationship to cancer cell fraction for single cell (model A, Red) and for the clonal model (model B, Blue). A*
 237 *sharp decrease in dN/dS at increasing CCF cut-offs consistent with the theoretical predictions for strong*
 238 *negative selection²¹. E) Immune dN/dS relationship to the probability of immune-mediated cell death at*
 239 *different levels of CCF. At low CCF, the dN/dS for model B is closer to one across all levels of immune death*
 240 *due to the presence of several undetected small frequency clones carrying neoantigens. At high CCF, both*
 241 *models show strong association between immune death and dN/dS. This results into cancer clones depleted*
 242 *of neoantigens, classified as immune-adapted and bearing an overall low tumor immunogenicity. F) Immune*
 243 *dN/dS at different CCF cut-offs when including escape mutations at 1% rate. At low CCF levels, immune*
 244 *dN/dS decreases when increasing CCF but escaped clones push the signal of immune dN/dS towards one*
 245 *at high CCF cut-offs for model B. G) Immune dN/dS relationship to the probability of immune-mediated cell*
 246 *death at different levels of CCF when escape mutations are included. For both models, increasing the*
 247 *probability of escape events pushes dN/dS values back to one for all CCF cut-offs, reflecting a relaxation of*

248 *immune-mediated negative selection. Ultimately, these tumors are growing with escape mechanisms that*
249 *allow the accumulation of neoantigens that increase the overall tumor immunogenicity.*

250

251 During the elimination phase, in addition to driver and passenger mutations, we
252 introduced immunogenic mutations (5% of immunogenic sites) and explored the
253 dynamics under two mechanisms of immune recognition (Single cell versus
254 clonal immune attack). We first calculated immune dN/dS values at different
255 cancer cell fraction (CCF) cutoffs. We observed that at increasing clone sizes the
256 immune dN/dS , and therefore tumor immunogenicity, value was approaching
257 zero for both models (Fig 2D). As in model B negative selection is absent for
258 small clones (low CCF), immune dN/dS was closer to 1. Then, we calculated
259 immune dN/dS at varying rates of immune-mediated cell death, P_{IS} , for different
260 clone sizes (Fig 2E). We first confirmed that when the immune system was
261 inactive ($P_{IS} = 0$), the immune dN/dS was one for all clones. At increasing levels
262 of effective immune surveillance both models demonstrated depletion of
263 immunogenic mutations, and therefore low levels of tumor immunogenicity.
264 Immune dN/dS in model B was less affected by this parameter given that multiple
265 immunogenic mutations can remain hidden at low frequency. Ultimately, these
266 simulations showed how immune dN/dS reveals the action of immune-mediated
267 negative selection and can be used as a proxy for tumor immunogenicity.

268

269 We next explored immune dN/dS values during the evolution of immune escape.
270 The activation of escape is modelled as a stochastic event occurring at a fixed
271 rate that depends on the proportion of escape sites in the genome. We repeated
272 simulations using an immune-mediated cell death of $P_{IS} = 1$ at different rates of
273 escape. We first found that when the proportion of escape sites was 1%, immune
274 dN/dS captured the action of immune-mediated negative selection across the
275 whole frequency spectrum (Fig 2F). In model B, immune escape pushed immune
276 dN/dS values back to one, slightly increasing overall tumor immunogenicity. At
277 higher rates of immune escape, we observed increased immune dN/dS
278 demonstrating how tumor immunogenicity is restored for all clone sizes when
279 escape events are more common (Fig 2G). Notably, when the escape rate was
280 5%, all clone sizes in model B reached immune dN/dS values close to one,

281 highlighting high levels of tumor immunogenicity. By acquiring escape
282 mechanisms, negative selection in the immunopeptidome is relaxed, the
283 accumulation of immunogenic mutations becomes neutral, and tumor
284 immunogenicity is restored.

285

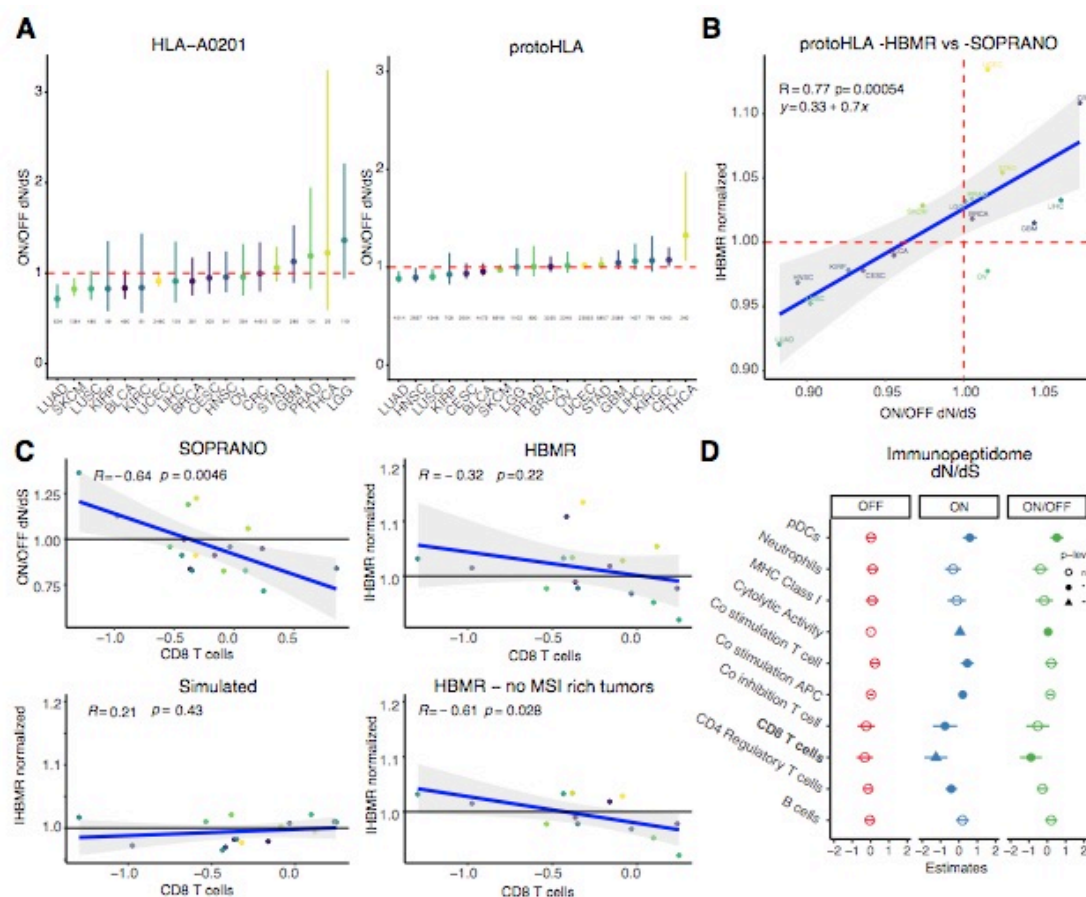
286 The results of our modelling provide a theoretical framework of co-evolution of
287 somatic cells and the immune system and a basis to quantify tumor
288 immunogenicity based on immune dN/dS . Further, it illustrates the importance of
289 choosing an appropriate region of the genome to analyse immune selection and
290 how clone sizes explain different levels of tumor immunogenicity. Moreover, we
291 speculate that when mixing patients that are immune-escaped with non-escaped,
292 signals of immune-mediated negative selection are no longer representative of
293 the overall tumor immunogenicity.

294

295 **High levels of lymphocyte infiltration are associated to strong immune-**
296 **mediated negative selection and low levels of tumor immunogenicity**

297 To measure global, driver, and immune dN/dS values using genomic data, we
298 developed SOPRANO (Selection On PRotein ANOtated regions), a bioinformatic
299 pipeline that measures the extent of selection in specific regions of the genome
300 (github.com/luisgls/SOPRANO). It extends our previous work, where we
301 calculated dN/dS corrected for mutational context using a 7-substitution type
302 (SSB7) or a 192-substitution model (SSB192)⁸. Here, we have extended the
303 method to account for any set of concatenated genomic regions allowing for
304 patient- and region- specific dN/dS estimates. We applied SOPRANO to 8543
305 tumour samples from 19 cancer types from The Cancer Genome Atlas (TCGA),
306 using the SSB192 model (Fig 3, Supplementary Table 2). We compared the ratio
307 of dN/dS values between regions inside and outside the immunopeptidome
308 (ON/OFF dN/dS). We defined the immunopeptidome as all possible wild-type 9-
309 mer regions present in the genome of a patient that are predicted to bind to the
310 MHC-I complex with an affinity of %rank < 0.5 as defined in netMHC4.0 (Fig S4).
311 In our first analysis, we used our previously published set of regions that bind to
312 HLA-A0201 and compared them to a recently published proto-HLA¹⁶ consisting

313 of multiple HLA alleles. We found that lung adenocarcinoma (LUAD) and
314 melanoma (SKCM) showed a depletion of nonsynonymous mutations in HLA-
315 A0201 binding regions, and that LUAD, HSNL and LUSC showed a depletion of
316 nonsynonymous mutations in proto-HLA regions (Fig 3A). We compared the
317 immune dN/dS values (ON/OFF dN/dS) obtained using SOPRANO to the values
318 of immune selection (normalized HLA-binding mutation ratio or HBMR), recently
319 reported by Van Den Eynden et al¹⁶. We observed a significant correlation
320 between the ON/OFF dN/dS ratio and the reported normalized HBMR using the
321 proto-HLA ($R=0.77$, P Value= 0.00054, Fig 3B) but not when comparing to the
322 HLA-A0201 ($R=0.37$, P Value= 0.15, Fig S5). Expectedly, the correlation for the
323 HLA-A0201 was lower given the HBMR value was calculated using multiple
324 HLAs- binding regions and therefore every patient not carrying the proto-HLA
325 allele will contribute with only neutrally accumulating mutations. In consequence,
326 it is important to note that the smaller the fraction of the assessed region that is
327 truly under immune selection, the more neutral the dN/dS value would appear.
328



329

330 *Figure 3. Immune dN/dS and immune activity across multiple tumor types. A) Immune dN/dS (ON/OFF dN/dS*
 331 *ratio) in multiple tumor types using either a curated HLA-A0201 target region or a proto-HLA consisting of*
 332 *the most common HLA haplotypes in the population obtained from Van Den Eynden et al¹⁶. Numbers*
 333 *represent the mutations ON target for each dataset. B) Comparison of immune dN/dS values using*
 334 *SOPRANO SSB-192 and normalized HBMR values reported in Van Den Eynden et al.¹⁶ C) Linear regression*
 335 *models for immune dN/dS and HBMR values versus median CD 8 T cell infiltration levels. In the analysis*
 336 *with no MSI-rich tumors, in addition to colorectal (CRC), we removed Stomach and Uterine cancer (STAD*
 337 *and UCEC). D) Linear mixed model using dN/dS values as the dependent variables and all immune metrics*
 338 *as independent variables. Model selection using AIC revealed that ON/OFF dN/dS is strongly associated to*
 339 *the levels of CD8 T cells. No immune value was associated to the global dN/dS (OFF).*

340

341 To determine whether immune-mediated negative selection was associated with
 342 levels of immune activity, we compared immune *dN/dS* to the levels of immune
 343 infiltration previously reported in TCGA data⁵¹ (Fig 3C). Median CD8 T cells
 344 significantly correlated to the SOPRANO-derived immune *dN/dS* values in HLA-
 345 A0201 regions ($p=0.0046$) but not to the HBMR values (proto-HLA) calculated in
 346 ¹⁶ ($p=0.22$), even though the trend was negative for both. As expected, the
 347 correlation was also not observed in the simulated dataset. Interestingly, when
 348 tumour types where microsatellite instability (MSI) and mismatch-repair
 349 deficiency was common, such as colorectal (CRC), stomach (STAD) and uterine
 350 cancer (UCEC), were excluded from the analysis, the correlation between proto-

351 HLA HBMR and the median CD8 T cells was significant ($P=0.028$), indicating that
352 negative selection acts differently in these different tumour subgroups. This
353 makes sense as hypermutant MSI tumours have a large frequency of escape
354 events, such as upregulation of immune checkpoint mechanisms, loss of
355 heterozygosity in the HLA region or mutations in genes associated to the antigen
356 presenting machinery^{28,33,52}. This last correlation was also strongly significant for
357 cytolytic activity (P -value = $6e-04$, Fig S6).

358

359 We applied a linear mixed model to determine the contribution to the global dN/dS
360 (OFF), the immunopeptidome-specific (ON) and the immune- dN/dS (ON/OFF)
361 using reported immune variables (Fig 3D). We performed a stepwise model
362 selection, and the initial (Fig S7) and best performing model for predicting
363 Immune dN/dS (R -square adj= 0.89, AIC= -83, p -value = 0.01) had CD8 T cells
364 as the most significant explanatory variable. Importantly, none of the variables
365 could explain global dN/dS values and seven out of the ten variables tested was
366 significantly associated to the immunopeptidome-specific ON value. Moreover,
367 we found that there was no significant correlation between CD8 T cells and
368 immune dN/dS in patients that have a truncating mutation in a gene associated
369 to the antigen presenting machinery or genes defined as escape genes
370 previously³⁴.

371

372 In summary, these results highlight the importance of considering multiple
373 confounding factors when drawing conclusions about the absence of negative
374 selection at the cohort level using dN/dS . These results further suggest that high
375 mutation burden tumors show signals of relaxed immune-selection confounding
376 the calculation and interpretation of dN/dS probably due to the presence of
377 acquired escape mechanisms, as our theoretical model predicts.

378

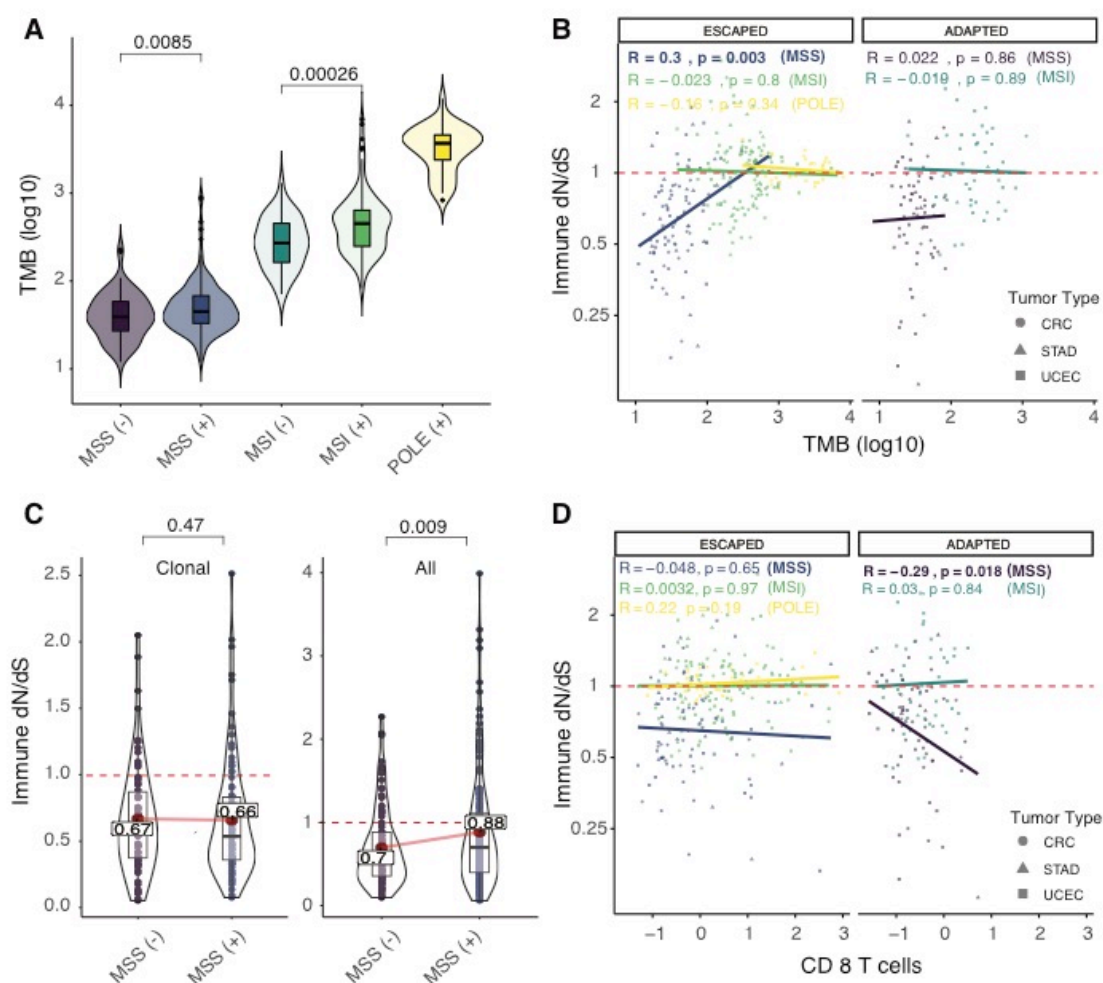
379 **Immune-escaped tumors show relaxed immune-mediated negative** 380 **selection and high tumor immunogenicity**

381 Following our immunoediting model, we hypothesized that escape events mask
382 the signal of immune mediated negative selection and restore tumor

383 immunogenicity. We ran SOPRANO using a patient specific immunopeptidome
384 (private HLA alleles) in colorectal (CRC), stomach (STAD) and uterine cancers
385 (UCEC). While tumor mutation burden was expectedly higher for MSI and POLE
386 tumors⁵³ (Fig S8), ON-target immunopeptidome dN/dS values for MSI and POLE
387 subtypes were also higher than for MSS tumors (Fig S9), consistent with high-
388 mutation rate tumours being very frequently immune-escaped²⁸.

389

390 We then classified different escape mechanisms for these tumors based on
391 previous work²⁸. We found that immune-escaped (Escape+) tumors have
392 significantly more somatic mutations compared to non-escaped (immune
393 adapted) tumors (MSS $p=0.0085$ and MSI $p=0.00026$, Fig 4A). We then reasoned
394 that a larger number of mutations in MSS escape+ tumors would push immune
395 dN/dS towards 1, given an extended time of neutral mutations accumulating in
396 the genome *after* immune escape has occurred. Indeed, we found a significant
397 positive correlation between tumor mutation burden and immune dN/dS for MSS
398 escape+ tumors but not for immune adapted tumors (Escape-, $p=1e-04$, Fig 4B),
399 suggesting that immune selection was still active in patients without an escape
400 mechanism. We observed the same results when restricting our analysis to only
401 clonal mutations (P Value = 0.003, Fig S10), confirming our previous suggestion
402 that immune-escape tends to occur early in the genesis of these malignancies²⁸.



403

404 *Figure 4. Patient specific analysis of colorectal (CRC), stomach (STAD) and uterine cancer (UCEC) using*
 405 *immune dN/dS. A) Tumor mutation burden (TMB) for different subtypes of cancers, including Microsatellite*
 406 *Stable (MSS), Microsatellite Instable (MSI) and POLE mutants, classified as immune-adapted (-) or immune-*
 407 *escaped (+) based on the presence of escape mechanisms (obtained from Lakatos et al²⁸). B) Relationship*
 408 *between Immune dN/dS values to TMB, following the same classification for patients as in A. C) Comparison*
 409 *between immune dN/dS values for immune-escaped and immune-adapted MSS tumors using all or only*
 410 *clonal mutations. D) Relationship between immune dN/dS values and the reported CD 8 T cell infiltration*
 411 *following the same classification for patients as in A and B.*

412

413 Our theoretical model predicted that immune *dN/dS* will remain lower than one
 414 when at large clone sizes in non-escaped patients. We expected that clonal
 415 mutations may still hold the signature of negative selection (active before escape)
 416 while subclonal mutations would be freely accumulating in immune-escaped
 417 tumors. Consequently, when we compared immune *dN/dS* between immune-
 418 adapted (escape-) and immune-escaped (escape+) MSS tumors, we observed
 419 that immune-escaped tumors had immune *dN/dS* values significantly closer to 1
 420 compared to immune-adapted tumors when using all mutations, but not when
 421 using clonal mutations (0.88 versus 0.7, Wilcoxon signed rank test=0.0009, Fig

422 4C). In the case of immune-adapted tumors, the Immune dN/dS when using all
423 or clonal mutations remained similar (0.68 versus 0.70 immune dN/dS) while
424 immune-escaped tumors had a significantly higher immune dN/dS when using all
425 mutations (0.88 versus 0.66 immune dN/dS , P Value=0.007) (Fig S11).

426

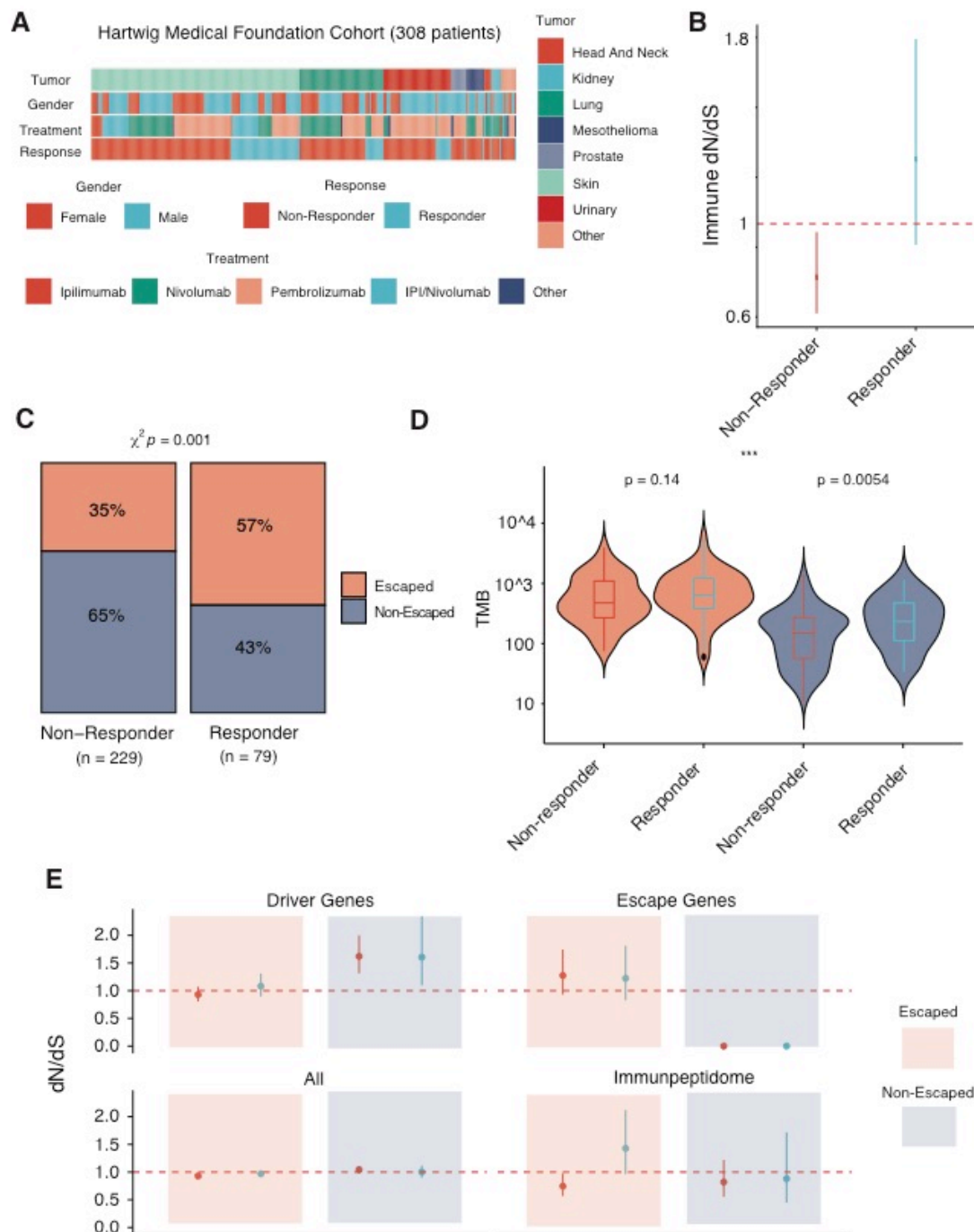
427 To validate that the strength of immune-mediated negative selection depends on
428 immune activity, we compared the patient specific immune dN/dS to the CD8 T
429 cell infiltration (Fig 4D). We found a significant association between immune
430 activity and CD8 T cells in immune-adapted MSS tumors (P Value = 0.018),
431 reaffirming that native HLA binding regions hold information on the strength of
432 immune selection elicited by CD 8 T cells. Interestingly, MSI tumors without an
433 annotated escape mechanism did not follow this pattern suggesting that these
434 tumors may have an unknown escape mechanism. These results highlight the
435 importance of understanding the evolutionary dynamics of tumors under
436 immunoediting and provide a theoretical explanation of why tumors with high
437 mutation burden are better candidates for immunotherapy. Such tumors have an
438 overall higher tumor immunogenicity that can be quantified using dN/dS in the
439 immunopeptidome.

440

441 **Immune-escaped tumors have better response to immunotherapy than** 442 **immune-adapted tumors**

443 To finally address the clinical importance of escape mutations and immune dN/dS
444 as a surrogate of tumor immunogenicity, we analysed 308 metastatic cases
445 subjected to immunotherapy with checkpoint inhibitors mainly with Ipilimumab,
446 Nivolumab, Ipi+Nivo, and Pembrolizumab from the Hartwig Medical Foundation
447 cohort⁴ (Fig 5A). The specimens were sequenced before treatment was started.
448 Following RECIST guidelines patients were classified into complete and partial
449 response and into progressive or stable disease (Methods). There were 78
450 responders recorded (Partial or complete response) and 229 non-responders
451 (Progressive or Stable disease). Due to the unavailability of patient specific HLA,
452 we calculated immune dN/dS using HLA-A0201 and observed a lower immune
453 dN/dS for non-responders compared to responders, suggesting that patients with

454 no response to immunotherapy were already adapted to the action of immune
455 response (Fig 5B). Next, we assembled a list of escape genes associated to the
456 immune response and further classified patients into immune-escaped and non-
457 escaped (Methods). Given that only genomic data was available for this cohort,
458 we could only classify patients into genetic escape and not into other immune
459 evasion events, such as overexpression of immune checkpoint inhibitors. We
460 found that the proportion of responders with a genetic escape mechanism was
461 significantly higher compared to non-responders (Chi-square P value = 0.001,
462 Fig 5C), indicating that escape mechanisms were independently associated to
463 the clinical response during immune checkpoint therapy.



464

465 *Figure 5. Analysis of Hartwig Medical Foundation metastatic cohort under immunotherapy. A) 308 patients*
 466 *with information about their response post-immunotherapy were selected. B) Immune dN/dS values for*
 467 *responders and non-responders reveals immune dN/dS lower than one for non-responders consistent with*
 468 *an overall tumor immunogenicity unresponsive to immunotherapies. C) Proportion of escaped and non-*
 469 *escaped tumors classified by clinical response. Responders are enriched in genetic escape mechanisms.*
 470 *D) Tumor mutation burden (TMB) for escaped and non-escaped tumors classified by response status.*
 471 *Among non-escaped patients, responders have a higher TMB than non-responders. E) dN/dS values for*
 472 *driver genes (196 genes from Martincorena et al ⁷), escape genes, all the exome and for the*
 473 *immunopeptidome. The panel show positive selection in driver genes for escaped tumors but not for non-*
 474 *escaped tumors. dN/dS in escape genes was indicative of positive selection for escaped tumors. Non-*
 475 *escaped tumors were selected for not having non-synonymous mutations in escape genes, hence dN/dS*
 476 *was 0. Global dN/dS values were one for all cases consistent with the lack of selection in the majority of the*
 477 *coding genome. dN/dS in the immunopeptidome was indicative of immune-selection for all groups except*
 478 *for escaped tumors in responders.*

479 Given that tumor mutation burden (TMB) is the current FDA-approved prognostic
480 marker of immunotherapy, we compared TMB between responders and non-
481 responders. As expected, we found that responders had a significantly higher
482 TMB than non-responders before the treatment (Fig S12A, P-value = 9.8×10^{-6} , U
483 Mann Whitney). In parallel, we looked at TMB between escape and non-escaped
484 patients and found that escaped patients had also a significantly higher TMB
485 compared to non-escaped (Fig S12B, P-Value < 2.2×10^{-16} , U Mann Whitney). We
486 also explored if TMB was different within escaped and non-escaped groups
487 separated by response. We found that TMB was significantly higher for
488 responders among the non-escaped group (P Value=0.0054, U Mann Whitney)
489 but not different among escaped patients (P value=0.14, U Mann Whitney) (Fig
490 5D). The fact that, among non-escaped patients, responders had higher TMB,
491 suggest that a group of responders had an escape mechanism that was not
492 considered in our classification. This is expected given that we did not consider
493 all possible escape mechanisms such loss of HLA heterozygosity³³, epigenetic
494 escape such as transcriptional silencing by changes in methylation³⁴, or extrinsic
495 factors such as the accumulation of dysfunctional T cells⁵⁴, all mechanisms of
496 immune evasion recently described in the literature.

497

498 Finally, we calculated dN/dS for driver, global, escape, and immune regions in
499 these four groups (Fig 5E). We found that the driver dN/dS was positive for non-
500 escaped tumors as expectedly, but surprisingly neutral for immune-escaped
501 tumors. The escape dN/dS showed signals of positive selection for escaped
502 patients and given that no nonsynonymous escape mutations were present in
503 non-escaped patients, the escape dN/dS was zero. The global dN/dS was
504 consistently close to one for all groups. Importantly, among escaped patients,
505 while the TMB was not different between responders and non-responders (Fig
506 5D), the immune dN/dS of non-responders was lower than one and lower than
507 the immune dN/dS of responders. Ultimately, this validates immune-adaptation
508 in non-responders showing less neoantigens and therefore low levels of tumour
509 immunogenicity for immunotherapies to have an effect.

510

511 Overall, our results highlight the importance of properly stratifying patients based
512 on escape mechanisms and immune dN/dS for a correct interpretation of the
513 evolutionary dynamics of tumors. In the future, these genomic based
514 classification in combination with current standard practices, could be used as
515 prognostic biomarkers for checkpoint inhibitor immunotherapies⁵⁵.

516

517 **Discussion**

518 The remarkable clinical response demonstrated by immune checkpoint inhibitors
519 (ICIs) has led to a growing interest in understanding the interactions between
520 cancer and immune cells^{33,35,56–58}. Although immunoediting is widely recognized
521 as an evolutionary process that selects for clones with low immunogenicity or
522 clones with an escape mechanism, its dynamics in the context of carcinogenesis
523 and response to treatment are poorly understood. During immunoediting, growing
524 cells are subjected to immune-mediated negative selection, shaping the
525 landscape of mutations observed in cancer. However, negative selection in
526 cancer has been a controversial topic^{10,15,16}. While some studies have shown
527 evidence of an association between immune activity and selective
528 pressures^{8,34,51,56,59}, others have claimed that there is a lack of evidence to prove
529 this relationship¹⁶. Given that several studies have applied dN/dS as a metric of
530 selection in cancer and in normal tissue^{7,8,60–63}, we aimed to prove the use of
531 dN/dS in the immunopeptidome as a proxy of tumor immunogenicity and as a
532 potential biomarker of immunotherapeutic response. In brief, we show that
533 immune dN/dS quantifies the extent of negative selection exerted by the immune
534 system and how levels of tumor immunogenicity measured by immune dN/dS can
535 be used as a genomic biomarker for response to immunotherapy.

536

537 We first show the evolutionary dynamics of tumorigenesis under two radically
538 different outcomes of immunoediting, immune-adaptation and immune-escape.
539 Such distinction is a key feature of cancer evolution and has profound clinical
540 implications. Immune-adapted tumors can only emerge in tissues where the
541 immune system can exert a selective pressure, suggesting that tissues with a
542 high capacity of immune recognition (immune-competent) are more likely to

543 generate clones with a depletion of immunogenic mutations if the probability of
544 escape is low (i.e. a low mutation rate). A lower number of neoantigens could
545 allow tumors to grow in both low and high immunogenic tissues, potentially
546 making them more aggressive when colonizing new niches. Supporting our
547 hypothesis, a recent study of longitudinal recurrence of metastasis reported a
548 more aggressive phenotype in metastatic deposits that had higher levels of
549 immune-selection⁵⁶. However, whether tumor cells growing in immune-
550 competent tissues are more likely to colonize new niches and how long it takes
551 those tumor cells to readapt or to find a novel escape mechanism, as has been
552 previously observed in mice models^{29,31,50}, remains a challenging question.

553

554 Our immunoediting model predicts that immune-adapted tumours have an overall
555 low tumor immunogenicity and will be less likely to respond to ICIs regardless of
556 tumor mutation burden status (TMB). TMB has been regarded as a measure of
557 tumor immunogenicity and is the current FDA-approved prognostic biomarker
558 used to enrol patients for ICI treatment. However, TMB does not capture the full
559 evolutionary history of the tumor and several patients do not respond despite their
560 TMB status. In addition, a recent study has shown that mismatch repair-proficient
561 colorectal cancers can also achieve clinical response⁴⁴. Motivated by this, we
562 propose that immune dN/dS can be used, in addition to TMB and escape
563 mechanisms, to stratify patients into adapted and escaped. As evidence of this,
564 we demonstrate that in a metastatic cohort, non-responders have an immune
565 dN/dS lower than one prior to immunotherapy and are thus immune-adapted,
566 whereas responders have immune dN/dS values of one, and are more likely to
567 be immune-escaped.

568

569 In conclusion, our study reflects the importance of understanding the evolutionary
570 dynamics of immunoediting during tumor evolution and how immune selection
571 edits the genome of tumor cells. Differentiating between immune adapted and
572 immune escaped tumors is a key factor when predicting which patients will benefit
573 from immunotherapies. In the future, we believe that immune dN/dS can be used

574 as read-out of tumor immunogenicity, that, in combination with other prognostic
575 measurements, can be used to predict response to immunotherapy.

576

577 References

-
- 578 1. Nowell, P. C. The clonal evolution of tumor cell populations. *Science (80-.)*. **194**, 23–28 (1976).
- 579 2. Greaves, M. & Maley, C. C. Clonal evolution in cancer. *Nature* **481**, 306–313 (2012).
- 580 3. Stratton, M. R., Campbell, P. J. & Futreal, P. A. The cancer genome. *Nature* **458**, 719–724 (2009).
- 581 4. Priestley, P. *et al.* Pan-cancer whole-genome analyses of metastatic solid tumours. *Nature* **575**, 210–216
582 (2019).
- 583 5. Martincorena, I. *et al.* Somatic mutant clones colonize the human esophagus with age. *Science (80-.)*. **362**,
584 911–917 (2018).
- 585 6. Yokoyama, A. *et al.* Age-related remodelling of oesophageal epithelia by mutated cancer drivers. *Nature* **565**,
586 312–317 (2019).
- 587 7. Martincorena, I., Raine, K. M., Davies, H., Stratton, M. R. & Campbell, P. J. Universal Patterns of Selection in
588 Cancer and Somatic Tissues. *Cell* **171**, 1029–1041.e21 (2017).
- 589 8. Zapata, L. *et al.* Negative selection in tumor genome evolution acts on essential cellular functions and the
590 immunopeptidome. *Genome Biol.* **19**, 67 (2018).
- 591 9. Weghorn, D. & Sunyaev, S. Bayesian inference of negative and positive selection in human cancers. *Nat*
592 *Genet* **49**, 1785–1788 (2017).
- 593 10. López, S. *et al.* Interplay between whole-genome doubling and the accumulation of deleterious alterations in
594 cancer evolution. *Nat. Genet.* **52**, 283–293 (2020).
- 595 11. Davis, A., Gao, R. & Navin, N. Tumor evolution: Linear, branching, neutral or punctuated? *Biochim. Biophys.*
596 *Acta - Rev. Cancer* **1867**, 151–161 (2017).
- 597 12. Williams, M. J., Werner, B., Barnes, C. P., Graham, T. A. & Sottoriva, A. Identification of neutral tumor
598 evolution across cancer types. *Nat Genet* **48**, 238–244 (2016).
- 599 13. Heide, T. *et al.* Reply to ‘Neutral tumor evolution?’ *Nat. Genet.* **50**, 1633–1637 (2018).
- 600 14. Tarabichi, M. *et al.* Neutral tumor evolution? *Nat. Genet.* **50**, 1630–1633 (2018).
- 601 15. Bakhoun, S. F. & Landau, D. A. Cancer Evolution: No Room for Negative Selection. *Cell* **171**, 987–989 (2017).
- 602 16. Van den Eynden, J., Jiménez-Sánchez, A., Miller, M. L. & Larsson, E. Lack of detectable neoantigen depletion
603 signals in the untreated cancer genome. *Nat. Genet.* **51**, 1741–1748 (2019).
- 604 17. Nordling, C. O. A new theory on the cancer-inducing mechanism. *Br. J. Cancer* **7**, 68 (1953).
- 605 18. Tomasetti, C., Marchionni, L., Nowak, M. A., Parmigiani, G. & Vogelstein, B. Only three driver gene mutations
606 are required for the development of lung and colorectal cancers. *Proc Natl Acad Sci U S A* **112**, 118–123
607 (2015).
- 608 19. Temko, D., Tomlinson, I. P. M., Severini, S., Schuster-Böckler, B. & Graham, T. A. The effects of mutational
609 processes and selection on driver mutations across cancer types. *Nat. Commun.* **9**, (2018).
- 610 20. Williams, M. J. *et al.* Quantification of subclonal selection in cancer from bulk sequencing data. *Nat. Genet.* 1–9
611 (2018). doi:10.1038/s41588-018-0128-6
- 612 21. Williams, M. J. *et al.* Measuring the distribution of fitness effects in somatic evolution by combining clonal
613 dynamics with dN/dS ratios. *Elife* **9**:e48714, 661264 (2020).
- 614 22. Watson, C. J. *et al.* The evolutionary dynamics and fitness landscape of clonal hematopoiesis. *Science (80-.)*.
615 **367**, 1449–1454 (2020).
- 616 23. McFarland, C. D., Korolev, K. S., Kryukov, G. V., Sunyaev, S. R. & Mirny, L. A. Impact of deleterious passenger
617 mutations on cancer progression. *Proc Natl Acad Sci U S A* **110**, 2910–2915 (2013).
- 618 24. McFarland, C. D., Mirny, L. A. & Korolev, K. S. Tug-of-war between driver and passenger mutations in cancer
619 and other adaptive processes. *Proc Natl Acad Sci U S A* **111**, 15138–15143 (2014).

- 620 25. Van den Eynden, J. & Larsson, E. Mutational Signatures Are Critical for Proper Estimation of Purifying
621 Selection Pressures in Cancer Somatic Mutation Data When Using the dN/dS Metric. *Front Genet* **8**, 74
622 (2017).
- 623 26. Persi, E., Wolf, Y. I., Leiserson, M. D. M., Koonin, E. V & Ruppin, E. Criticality in tumor evolution and clinical
624 outcome. *Proc. Natl. Acad. Sci. U. S. A.* **115**, E11101–E11110 (2018).
- 625 27. Pyatnitskiy, M., Karpov, D., Poverennaya, E., Lisitsa, A. & Moshkovskii, S. Bringing Down Cancer Aircraft:
626 Searching for Essential Hypomutated Proteins in Skin Melanoma. *PLoS One* **10**, e0142819 (2015).
- 627 28. Lakatos, E. *et al.* Evolutionary dynamics of neoantigens in growing tumours. *bioRxiv* 536433 (2019).
628 doi:10.1101/536433
- 629 29. Dunn, G. P., Bruce, A. T., Ikeda, H., Old, L. J. & Schreiber, R. D. Cancer immunoediting: from
630 immunosurveillance to tumor escape. *Nature Immunology* **3**, 991–998 (2002).
- 631 30. Dunn, G. P., Old, L. J. & Schreiber, R. D. The immunobiology of cancer immunosurveillance and
632 immunoediting. *Immunity* **21**, 137–148 (2004).
- 633 31. Schreiber, R. D., Old, L. J. & Smyth, M. J. Cancer immunoediting: Integrating immunity's roles in cancer
634 suppression and promotion. *Science (80-.)*. **331**, 1565–1570 (2011).
- 635 32. Matsushita, H. *et al.* Cancer exome analysis reveals a T-cell-dependent mechanism of cancer immunoediting.
636 *Nature* **482**, 400–404 (2012).
- 637 33. McGranahan, N. *et al.* Allele-Specific HLA Loss and Immune Escape in Lung Cancer Evolution. *Cell* **171**,
638 1259-1271.e11 (2017).
- 639 34. Rosenthal, R. *et al.* Neoantigen-directed immune escape in lung cancer evolution. *Nature* **567**, 479–485
640 (2019).
- 641 35. Chowell, D. *et al.* Evolutionary divergence of HLA class I genotype impacts efficacy of cancer immunotherapy.
642 *Nat. Med.* doi:10.1038/s41591-019-0639-4
- 643 36. Bräunlein, E. & Krackhardt, A. M. Identification and Characterization of Neoantigens As Well As Respective
644 Immune Responses in Cancer Patients. *Front. Immunol.* **8**, 1–8 (2017).
- 645 37. Fritsch, E. F. *et al.* HLA-binding properties of tumor neopeptides in humans. *Cancer Immunol. Res.* **2**, 522–529
646 (2014).
- 647 38. Charoentong, P. *et al.* Pan-cancer Immunogenomic Analyses Reveal Genotype-Immuno-phenotype
648 Relationships and Predictors of Response to Checkpoint Blockade. *Cell Rep.* **18**, 248–262 (2017).
- 649 39. Bindea, G. *et al.* Spatiotemporal dynamics of intratumoral immune cells reveal the immune landscape in
650 human cancer. *Immunity* **39**, 782–795 (2013).
- 651 40. Galon, J. *et al.* Towards the introduction of the 'Immunoscore' in the classification of malignant tumours. *J*
652 *Pathol* **232**, 199–209 (2014).
- 653 41. Quezada, S. A., Peggs, K. S., Simpson, T. R. & Allison, J. P. Shifting the equilibrium in cancer immunoediting:
654 From tumor tolerance to eradication. *Immunol. Rev.* **241**, 104–118 (2011).
- 655 42. Gajewski, T. F., Schreiber, H. & Fu, Y.-X. Innate and adaptive immune cells in the tumor microenvironment.
656 *Nat Immunol* **14**, 1014–1022 (2013).
- 657 43. Dupage, M., Mazumdar, C., Schmidt, L. M., Cheung, A. F. & Jacks, T. Expression of tumour-specific antigens
658 underlies cancer immunoediting. *Nature* **482**, 405–409 (2012).
- 659 44. Chalabi, M. *et al.* Neoadjuvant immunotherapy leads to pathological responses in MMR-proficient and MMR-
660 deficient early-stage colon cancers. *Nat. Med.* (2020). doi:10.1038/s41591-020-0805-8
- 661 45. Durrett, R. *Branching Process Models of Cancer Multistage theory of cancer.* (Springer International
662 Publishing, 2015). doi:10.1007/978-3-319-16065-8_1
- 663 46. Gatenbee, C. *et al.* Macrophage-mediated immunoediting drives ductal carcinoma evolution: Space is the
664 game changer. *bioRxiv* 594598 (2019). doi:10.1101/594598
- 665 47. Williams, M. J., Sottoriva, A. & Graham, T. A. Measuring Clonal Evolution in Cancer with Genomics. *Annu.*
666 *Rev. Genomics Hum. Genet.* **20**, (2019).
- 667 48. Gejman, R. S. *et al.* Rejection of immunogenic tumor clones is limited by clonal fraction. *Elife* **7**, 1–22 (2018).

- 668 49. Yang, Z. & Nielsen, R. Estimating synonymous and nonsynonymous substitution rates under realistic
669 evolutionary models. *Mol Biol Evol* **17**, 32–43 (2000).
- 670 50. Koebel, C. M. *et al.* Adaptive immunity maintains occult cancer in an equilibrium state. *Nature* **450**, 903–907
671 (2007).
- 672 51. Rooney, M. S., Shukla, S. A., Wu, C. J., Getz, G. & Hacohen, N. Molecular and genetic properties of tumors
673 associated with local immune cytolytic activity. *Cell* **160**, 48–61 (2015).
- 674 52. Le, D. T. *et al.* PD-1 Blockade in Tumors with Mismatch-Repair Deficiency. *N. Engl. J. Med.* **372**, 2509–2520
675 (2015).
- 676 53. Loupakis, F. *et al.* Prediction of Benefit from Checkpoint Inhibitors in Mismatch Repair Deficient Metastatic
677 Colorectal Cancer: Role of Tumor Infiltrating Lymphocytes. *Oncologist* **25**, 481–487 (2020).
- 678 54. Ghorani, E. *et al.* The T cell differentiation landscape is shaped by tumour mutations in lung cancer. *Nat.*
679 *Cancer* **1**, 546–561 (2020).
- 680 55. Havel, J. J., Chowell, D. & Chan, T. A. The evolving landscape of biomarkers for checkpoint inhibitor
681 immunotherapy. *Nat. Rev. Cancer* **19**, 133–150 (2019).
- 682 56. Angelova, M. *et al.* Evolution of Metastases in Space and Time under Immune Selection. *Cell* 1–15 (2018).
683 doi:10.1016/j.cell.2018.09.018
- 684 57. Zhang, A. W. *et al.* Interfaces of Malignant and Immunologic Clonal Dynamics in Ovarian Cancer. *Cell* **173**,
685 1755-1769.e22 (2018).
- 686 58. AbdulJabbar, K. *et al.* Geospatial immune variability illuminates differential evolution of lung adenocarcinoma.
687 *Nat. Med.* (2020). doi:10.1038/s41591-020-0900-x
- 688 59. Zhang, A. W. *et al.* Interfaces of Malignant and Immunologic Clonal Dynamics in Ovarian Cancer. *Cell* 1–15
689 (2018). doi:10.1016/j.cell.2018.03.073
- 690 60. Lee-Six, H. *et al.* The landscape of somatic mutation in normal colorectal epithelial cells. *Nature* **574**, 532–537
691 (2019).
- 692 61. Muyas, F., Zapata, L., Guigó, R. & Ossowski, S. The rate and spectrum of mosaic mutations during
693 embryogenesis revealed by RNA sequencing of 49 tissues. *Genome Med.* **12**, 1–19 (2020).
- 694 62. Benvenuto, M. *et al.* Tumor antigens heterogeneity and immune response-targeting neoantigens in breast
695 cancer. *Semin. Cancer Biol.* 1–12 (2019). doi:10.1016/j.semcancer.2019.10.023
- 696 63. Zacharakis, N. *et al.* Immune recognition of somatic mutations leading to complete durable regression in
697 metastatic breast cancer. *Nat. Med.* **24**, 724–730 (2018).
- 698 64. Caravagna, G. *et al.* Model-based tumor subclonal reconstruction. 1–31 (2019).
- 699 65. Fay, M. P. Two-sided exact tests and matching confidence intervals for discrete data. *R J.* **2**, 53–58 (2010).

700

701 Acknowledgements

702 L.Z. is supported by the European Union’s Horizon 2020 research and innovation
703 programme under the Marie Skłodowska-Curie Research Fellowship scheme
704 (846614). A.S. is supported by the Wellcome Trust (202778/B/16/Z) and Cancer
705 Research UK (A22909). We acknowledge funding from the National Institute of
706 Health (NCI U54 CA217376) to A.S. and T.G. This work was also supported by
707 a Wellcome Trust award to the Centre for Evolution and Cancer (105104/Z/14/Z).
708 We thank Claire-Alix Garin and Marco Punta for support and discussion. This
709 publication and the underlying study have been made possible partly on the basis

710 of the data that Hartwig Medical Foundation and the Center of Personalised
711 Cancer Treatment (CPCT) have made available to the study.

712

713 **Author contributions**

714 LZ conceived, designed, implemented and performed all analysis, GC supported
715 with the model implementation, MW, EL, and BW provided support with the
716 mathematical inferences of the model. KAJ provided bioinformatic support. TG
717 and AS supervised the project. LZ wrote the first draft of the manuscript. LZ, AS
718 and TG wrote the final version of the manuscript with the help of all the authors.

719

720 **Competing interests**

721 The authors declare no competing interests.

722

723 **Data availability**

724 TCGA data was obtained from GDC portal and processed as described in¹³.
725 Assembled list of escape mechanisms for COAD, READ and STAD and UCEC
726 was obtained from Lakatos et al²⁸. Hartwig Medical Foundation data was
727 downloaded from Hartwig Data Portal. HBMR values of selection in the
728 immunopeptidome were obtained from the supplementary material in Van Den
729 Eynden et al¹⁶. Normalized scores for immune cell infiltration was obtained from
730 Rooney et al⁵¹.

731

732 **Code Availability**

733 SOPRANO is freely available at github.com/luisgls/SOPRANO. Simulator of
734 stochastic branching process for immunoediting is available at
735 github.com/luisgls/dNdSSimulator upon request. All figures are available as a
736 markdown file.

737

738 **Methods**

739 **1.0 Evolutionary model of tumorigenesis under immunoediting**

740 **1.1 Computational model**

741 We have developed a discrete-time non-spatial stochastic branching process of
742 somatic evolution. It models the acquisition of somatic mutations and their
743 associated effect on the phenotype of single cells. The model can be initialized
744 with any number of wild-type single cells and a set of initial parameters described
745 in supplementary table 1A.

746

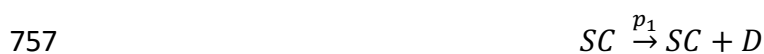
747 **1.2 Cell division process**

748 The model simulates cellular proliferation starting from x_0 identical initial cells
749 available at time $t_0 = 0$, that divide synchronously; each time-step therefore is
750 represented in units of tumour doublings or generations, as in earlier works⁴⁷.

751

752 At every time-step every single cell (SC) in the model undergoes a stochastic
753 process with a probability that depends on a parameter p_i . The outcomes of this
754 process are either zero, one, or two single cells in the model:

755



759

760 where $p_0 + p_1 + p_2 = 1$ and D denotes “dead” cells. We consider death as any
761 process that removes the cell from the dividing population, such as apoptosis,
762 senescence, quiescence, or differentiation. To simplify the possible outcomes of
763 the model, we consider $p_1 = 0$. Thus, our branching process consists only of no
764 division (no offspring) or a successful cell division (two daughter cells), that is
765 $p_0 + p_2 = 1$. Given that $p_0 = 1 - p_2$, we can define the probability of survival
766 $p_2 = \Delta$ as the parameter of fitness for each single cell. In the case of a neutral
767 branching process and at the initial state of the simulation (time t_0) the probability
768 of cell division is equal to the probability of cell death/differentiation for each single
769 cell ($\Delta = 0.5$).

770

771 We can translate this parameter Δ into a birth death process with $b/d = \omega$ using:

772

773
$$\omega = 2 * p2 + 1 * p1 + 0 * p0$$

774
$$\omega = 2 * \Delta$$

775 [2]

776
$$\omega = b/d$$

777
$$b/d = 2 * \Delta$$

778

779 when $\Delta = 0.5$ the birth death ratio $b/d = 1$.

780

781 The population grow exponentially when the probability of division (Δ) is 1. The
782 probability of survival Δ used as a phenotype allow us to define a driver clone. A
783 driver clone is a set of cells from the same evolutionary lineage which have the
784 same Δ across them. This implies that they all have a shared set of mutations
785 (very few or all) and the same survival probability. We also define an
786 immunogenic clone, defined by the presence of an ancestral cell that acquired at
787 least one immunogenic mutation.

788

789 **1.3 Cell genotypes and phenotypes.**

790

791 The genotype of each single cell is implemented as a vector storing the following
792 information:

793

-
- 794 • Number of nonsynonymous mutations in driver, immune, escape, and
795 passenger regions of the coding genome.
 - 796 • Number of synonymous mutations in driver, immune and passenger
797 regions of the coding genome.
-

798

799 At every successful cell division, each cell inherits the genotype from the parental
800 cell, which is further modified by acquiring a new set of mutations. The number
801 of new mutations is given by a Poisson distribution with mean $u * L$ with $L = 50 * 10^6$,
802 u is the mutation rate per bp per cell division, and L is the length of the
803 coding genome.

804

805 The phenotype of each single cell is implemented as a vector storing the following
806 information:

807

-
- 808 • Fitness (probability of successful cell division) and strategy (passenger,
809 driver, immunogenic or escape),
-

810

811 These phenotypes are the outcome of mutations present in the genotype vector.
812 To estimate the target size and thus the vector of probabilities for passenger,
813 driver, immunogenic, and escape mutations we used prior information and also
814 explored different values. All tested values are described in supplementary table
815 1B.

816

817 **1.4 Cycle conditions**

818 Our model requires the input of several parameters described in supplementary
819 Table 1. We performed several simulations to account for the different phases
820 described in figure 1. The parameters for the simulations are described in
821 supplementary table 1B.

822

823 **Mutation rate**

824 Specifically, for MSS cases, we used a mutation rate per pb per cell division of
825 10^{-8} . This value is a composite between the polymerase error and the DNA
826 proofreading correction efficiency. For MSI and POLE cases we increased this
827 value in one and two orders of magnitude respectively.

828

829 Initially, we estimated the probability of hitting a driver mutation (1%) based on
830 the number of driver genes identified in a recent study using a pancancer dataset
831 (~200 out of 20000 genes)⁷. We used 5% of the coding genome as immunogenic
832 based on our recent analysis of immunogenic mutations²⁸ and based on the
833 length of all possible 9-mers defined as strong binders by NetMHCpan. The
834 proportion of escape sites in the coding genome is unknown, thus we simulated
835 different proportions ranging from 0.01% to 5%. In addition, we defined
836 nonsynonymous mutations as: a) passenger mutations that do not have any

837 effect on the phenotype, b) driver mutations increasing the probability of survival,
838 c) immunogenic mutations that may elicit an immune response, d) escape
839 mutations allowing the cell to hide from an immune attack. We assume that all
840 synonymous mutations accumulate neutrally in the genome and define three
841 types of synonymous a) synonymous mutations in neutral regions, b) in driver
842 regions, and c) in the immunopeptidome. To simulate the dependency of the
843 nonsynonymous to synonymous mutation ratio, dN/dS values, for global, driver
844 and immune regions, we fixed the probability of synonymous mutations as 1/3 of
845 the probability of the nonsynonymous mutations in the same locus. All these
846 probabilities sum to one.

847

848 Then, each time a cell divides, each daughter cell inherits the parental genotype
849 and an additional set of nonsynonymous and synonymous mutations based on
850 the probability vector defined. Our model assumes infinite-sites and no -back
851 mutation as used in previous studies⁶⁴. Our model records the number of
852 mutations for each mutation type, the probability vector for each of those
853 mutations, the probability of survival and the probability of immune attack over
854 time. We also store the parental relationship and we assign a new clone id only
855 when the new genotype includes nonsynonymous driver different from the
856 parental phenotype.

857

858 We stopped the simulation after 100 generations, consistent with the maximum
859 number of cell divisions allowed by telomere shrinking, or when the population
860 size reached a specific carrying capacity (2000 cells).

861

862 **1.4 Mutation effects**

863 **Phenotype 1 - Proliferation dynamics**

864 We have developed a flexible framework to account for different models of fitness
865 effects of driver mutations. We chose a model based on that to date we have
866 mostly seen tumors having between 2-10 drivers, therefore at equilibrium we
867 expect to reach an average of 5 clones each carrying a driver event or 1 clone
868 carrying 5 driver events. Thus, we modelled the fitness increase by a driver event

869 as a Gompertz function where driver events give different selective advantages
870 based on the order of acquisition given by:

871

$$872 \quad S(d) = 0.5 * e^{-b * e^{-cd}}$$

873

874 where b defines the displacement scale parameter of the Gompertz function, c
875 defines the scale parameter on the fitness effect for each driver, and d is the
876 number of driver events. We sample b from a normal distribution with mean 5 and
877 c has a fixed value of 1.

878

879 Finally, at each time point each cell has a probability of survival defined by:

880

$$881 \quad \Delta = 0.5 + S(d)$$

882

883 We must emphasize that the choice on these functions is perhaps one of the
884 most important open questions in the field of cancer evolution. The fitness effects
885 of combinations of multiple drivers (epistasis), the proportion of mutated sites
886 leading to an increase/decrease of a selective advantage, and whether there is
887 an upper boundary for the fitness increase remain largely unsolved and it was
888 not the scope of this work. Here, we aimed to explore the effects of the immune
889 system, the selective pressures and the emergence of escape mutations on a
890 single unifying framework of tumor evolution.

891

892 **Phenotype 2 - Immunoediting:**

893 To model the effect of the immune system during somatic evolution we assume
894 two possible scenarios.

895

896 In the first, we allow cells to accumulate immunogenic mutations based on the
897 size of the immunogenic genome and the mutation rate. Each immunogenic
898 mutation will be detected by the immune system at an immune-mediated cell
899 death rate of P_{IS} that will remove the immunogenic cell. This rate can be seen as
900 the healthiness of the immune system or the capacity of T-cell recognition based

901 on the diversity of the TCR repertoire (with 0 for immunosuppressed to 1 for
902 immunocompetent, alternatively this can be seen as low recognition or high
903 recognition potential by TCRs). By simplifying this value to an external probability
904 independent of the genome, it allows us to model the effect of the
905 microenvironment.

906

907 In the second, we define a function that at every generation calculates how many
908 cells in a given clone are immunogenic (at least one neoantigen) and if this
909 number is greater than a selected cut-off value (50 cells in our model), we kill all
910 cells from that clone given a certain probability (defined previously as P_{IS}). An
911 immunogenic cell carries at least one immunogenic mutation and have not
912 acquired an escape mutation. When a cell acquires an escape mutation, the
913 immune system will no longer attack this cell.

914

915 **1.5 dN/dS computation**

916 To estimate the dN/dS ratio we fixed the initial probabilities of occurrence of
917 nonsynonymous mutations to be three times higher than the occurrence of
918 synonymous mutations, as naturally observed in the coding portion of the human
919 genome.

920

921 In general, in the first cellular divisions the number of synonymous mutations is
922 close to 0 for many cells making the calculation of dN/dS implausible (infinite).
923 We calculated the dN/dS for all mutations (global dN/dS), driver mutations (driver
924 dN/dS) and immunogenic mutations (immune dN/dS) by adding up the observed
925 counts in the alive cells at a given time t .

926

$$927 \quad \text{global} \quad \frac{dN}{dS} = \frac{\sum ns_passenger + \sum ns_driver + \sum ns_immunogenic + \sum ns_escape}{3 * (\sum s_passenger + \sum s_driver + \sum s_immunogenic + \sum s_escape)}$$

928

$$929 \quad \text{driver} \quad \frac{dN}{dS} = \frac{\sum ns_driver}{3 * \sum s_driver}$$

930

$$931 \quad \text{Immune} \quad \frac{dN}{dS} = \frac{\sum ns_immunogenic}{3 * \sum s_immunogenic}$$

932

933 **1.6 Frequency dN/dS**

934 To estimate the dN/dS ratio using a specific mutation frequency cut off we
935 simulated sequencing by giving a mutation ID to each new mutation acquired
936 during the stochastic branching process. We determine the cell-specific mutation
937 by implementing an algorithm that walks along the lineage of a cell and
938 concatenate all inherited mutations. We build a matrix of all alive cells and
939 mutations at the last time point. We then were able to filter out variants present
940 in less than any predefined threshold. For the driver section we used 0.01%, 1%,
941 2%, 3%, 4%, 5%, 10%, 25%, and 50% as frequency cut-offs. For the immune
942 section we used 0.1%, 1%, 5%, 10% and 50% as frequency cut-offs. To estimate
943 dN and dS we assigned each inherited mutation a unique id. Given that each
944 mutation has two labels, a first label defined as 1) nonsynonymous and
945 synonymous, and a second label defined as a 2) passenger, driver and
946 immunogenic. This allowed us to calculate a global, driver, and immune dN/dS
947 accordingly. Then, each simulation consisted of N number of cells with a specific
948 number of nonsynonymous and synonymous driver, immunogenic, and
949 passenger mutations.

950

951 **1.7 dN/dS confidence Intervals for frequency or cancer cell fraction cut-offs**

952 When performing the analysis using frequency cut-offs, we pulled simulations
953 together similar to what is done in cohort studies when all nonsynonymous and
954 synonymous mutations are pulled together. To estimate the confidence interval
955 for this analysis, we used the `rateratio.test` function from R package `rateratio`.
956 This function calculates the p-value and the confidence interval for the rate of two
957 Poisson ratios. It uses the uniformly most powerful ratio test available for R⁶⁵.

958

959 **2.0 TCGA Data**

960 We first obtained somatic calls of TCGA data from GDC. This dataset consisted
961 of 10202 samples across 33 tumors types. We then selected 19 tumor types
962 tumor types that had been analysed in Rooney et al⁵¹ in order to compare our
963 results of immune dN/dS to the immune cell scores. Rooney et al provided the
964 per patient values of several normalized scores for immune cells. We calculated

965 the median value for each score within each tumor type. The final list analysed
966 consisted of 8543 samples across 19 tumor types. TCGA data was then re-
967 annotated using ensembl-VEP release 89. COAD (Colon adenocarcinoma) and
968 READ (Rectum Adenocarcinoma) were merged into CRC.

969

970 HLA-binding Mutation Ratios (HBMR) and simulated HBMRs were obtained from
971 the supplementary material in Van Den Eynden et al¹⁶ available for 19 tumor
972 types. Hartwig somatic calls and metadata were obtained from Hartwig Medical
973 Foundation under license agreement DR-075.

974

975 **2.1 Selection On PRotein ANotated regiOns, SOPRANO**

976 SOPRANO was developed on top of the method developed in Zapata et al 2018
977 to calculate selection in VEP annotated files and is freely available in
978 github.com/luisgls/SOPRANO. It estimates dN/dS values in a target region (ON-
979 target) and in the rest of the proteome (OFF-target) using a trinucleotide context
980 correction (SSB192) or a 7-nucleotide context (SSB7). It allows the option to
981 include or exclude cancer driver genes, as well as, randomizing the target region
982 to calculate a background distribution of a matching size region. Given that it uses
983 a set of Ensembl transcript identifiers and their respective FASTA file it allows
984 calculation of dN/dS in any genome irrespective of the version. We ran
985 SOPRANO on 33 tumor types and deposited the results for each tumor type in
986 Synapse (syn22149238).

987

988 **2.2 Immunopeptidome and patient specific HLA**

989 We downloaded a set of protein coding transcripts with HGNC symbol from
990 Ensembl Biomart. We obtained all transcript lengths and run bedtools
991 makewindows to get all possible overlapping 9-mers. We then obtained the
992 FASTA sequence for each of all 9-mer and run netMHCpan4 using a list of HLA-
993 alleles. This list of HLA-alleles was restricted to those that have more than 1%
994 population frequency in a list of 1277 samples from the 1000K cohort. We
995 selected all possible strong binders which had a mean and a median expression

996 above 1FPKM. We obtained expression values for different tissues from the
997 human protein atlas (downloaded on 05/10/2018).

998

999 **3.0 Analysis of Metastatic cohort pre-immunotherapy from Hartwig Medical** 1000 **Foundation**

1001

1002 We obtained the somatic mutation data from the Hartwig Medical Foundation
1003 cohort (HMF) under license agreement DR-075. The data we used for this
1004 manuscript consisted on 308 metastatic patients that underwent immunotherapy
1005 post-biopsy and that had recorded clinical response in "first response" column
1006 from the metadata. Mutation types that were not classified as synonymous,
1007 missense, start_lost, stop gained, stop lost or frameshift mutation were excluded.
1008 We removed indels and reannotated SNVs following our pipeline to obtain high
1009 confidence calls for a predefined set of ensemble transcripts (~20000 genes). We
1010 then rerun ensemble VEP using version 90 for Grch37 and parse the file using
1011 VATools V1.0.0. We uploaded the final annotated file used for the rest of the
1012 manuscript for each of the 308 patients to Synapse.

1013

1014 It is important to note that the raw clinical data was supplied by HMF and final
1015 consistency checks are still to be performed. The response evaluations were not
1016 performed as part of a clinical trial and the timing of the evaluations was variable.
1017 We classified patients into responders and non-responders based on the first
1018 response recorded after treatment was initiated. The group of responders
1019 consisted of those that were labelled complete response (CR, 1 case), or partial
1020 response (PR, 78 cases). Those that were labelled stable diseases (SD, 98
1021 cases) or progressive disease (PD, 131 cases) were classified as non-
1022 responders. To keep consistency with other studies, there were 79 cases with no
1023 data, two cases classified as clinical progression, four cases classified as ND,
1024 and 3 cases classified as Non-CR/Non-PD which were not included in the
1025 analysis. The timing from biopsy to response was not included. There were no
1026 other further classifications performed.

1027

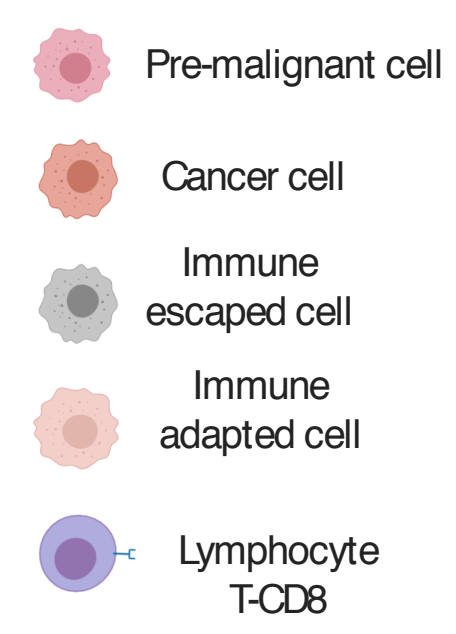
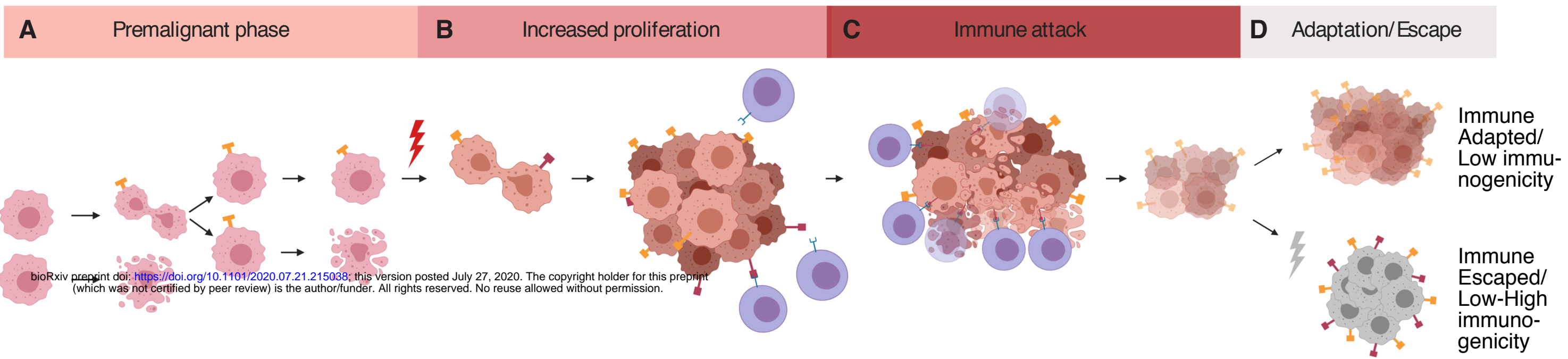
1028 Escape genes were selected based on the list of Antigen Processing and
1029 Presentation Machinery (hsa04612) download from KEGG. In addition, we
1030 included escape genes used in Rosenthal et al³⁴. We then classified responders
1031 and non-responders into "escaped" if there was a missense or a truncating
1032 mutation in one of these escape genes and into "adapted" otherwise.

1033

1034 All statistical tests were performed using R statistical language. Statistical tests
1035 were performed using Wilcoxon rank-sum test for two distributions or Kruskal-
1036 Willis test when more than two distributions were present using the R package
1037 ggstatsplot.

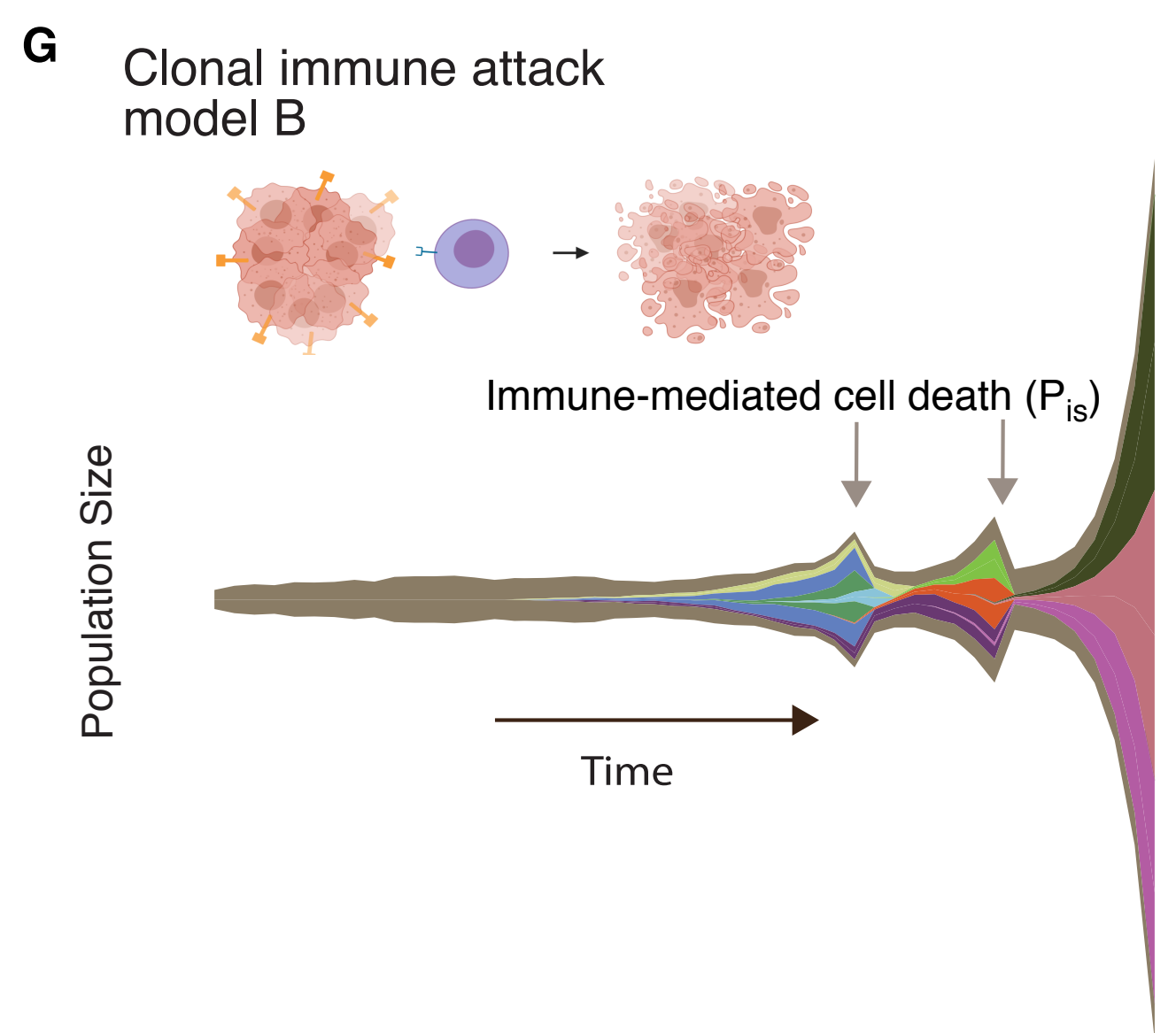
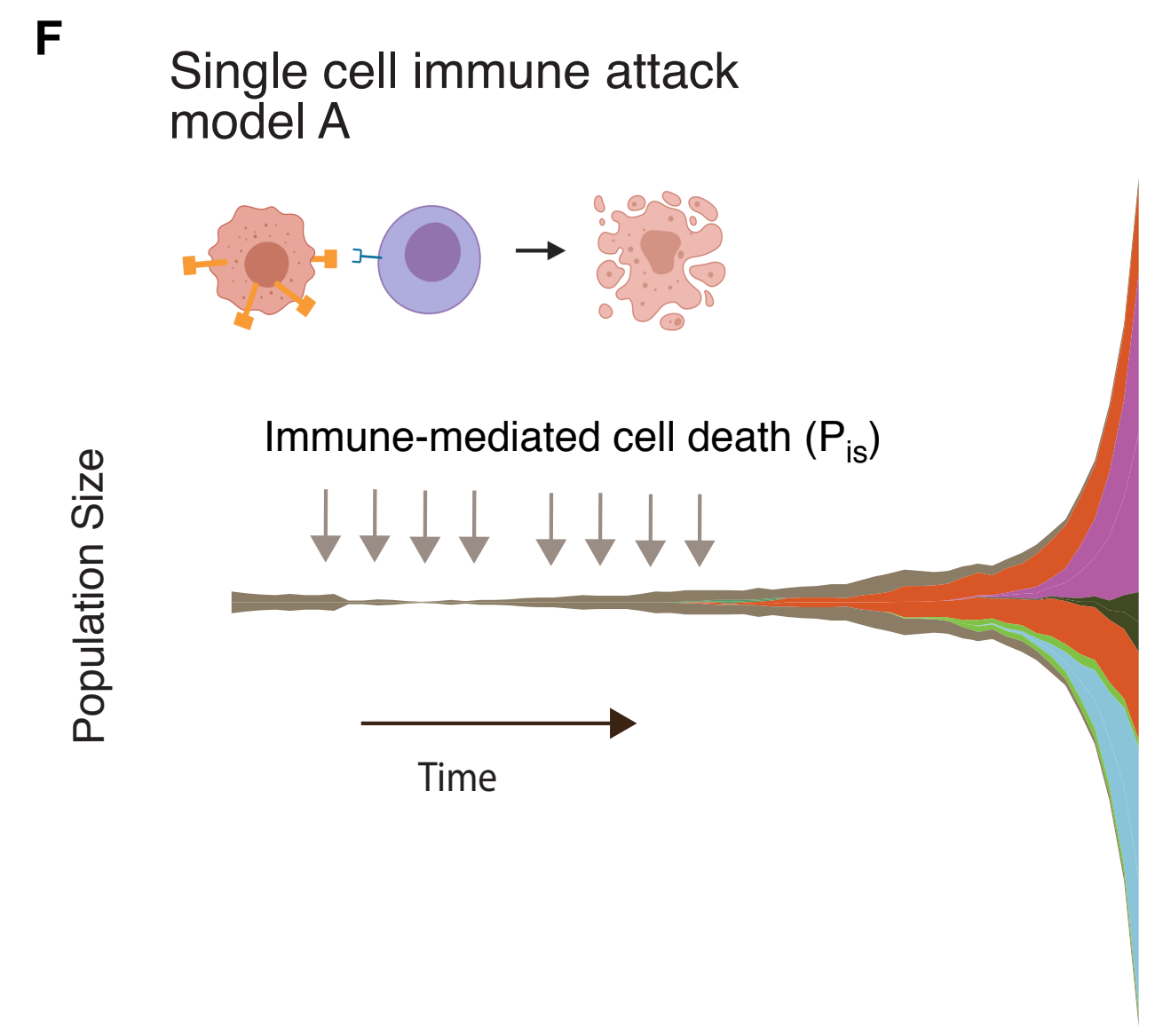
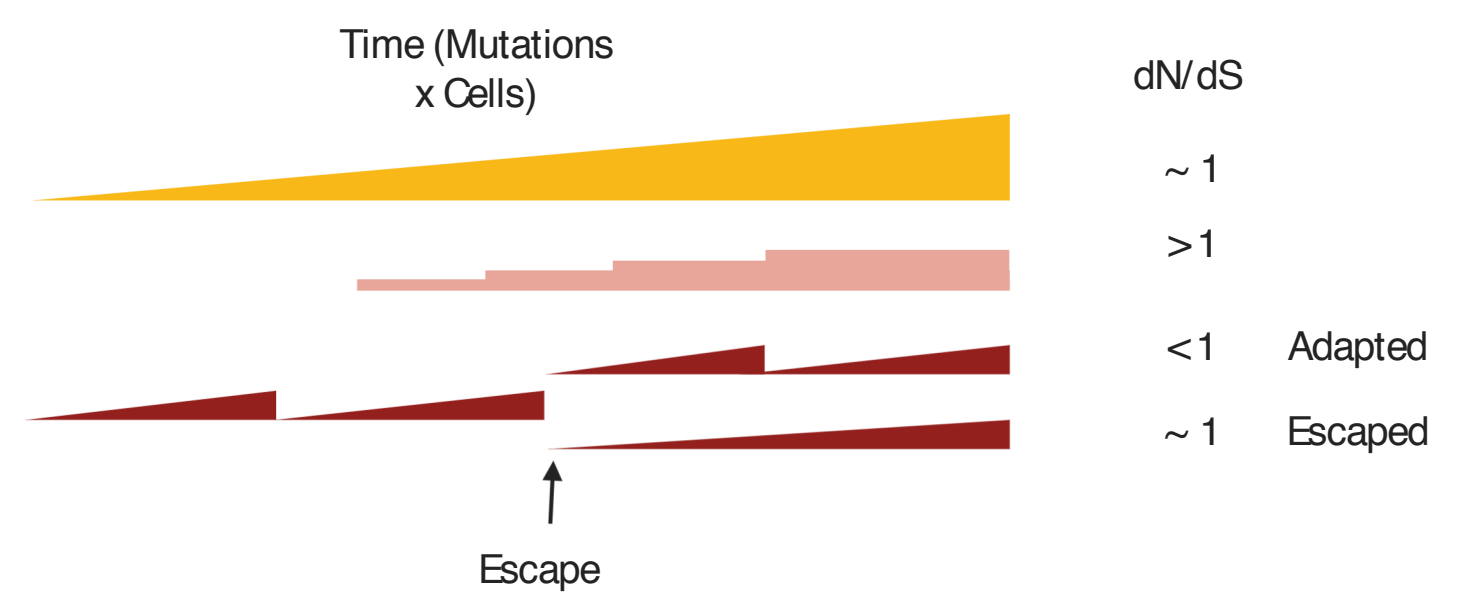
1038

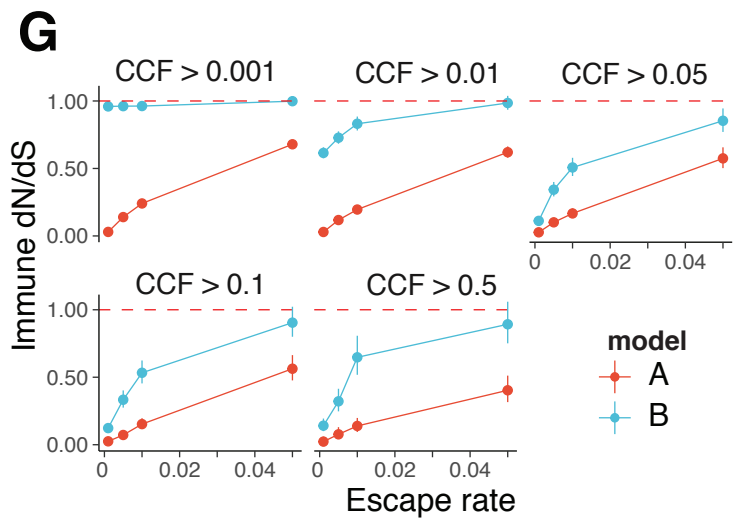
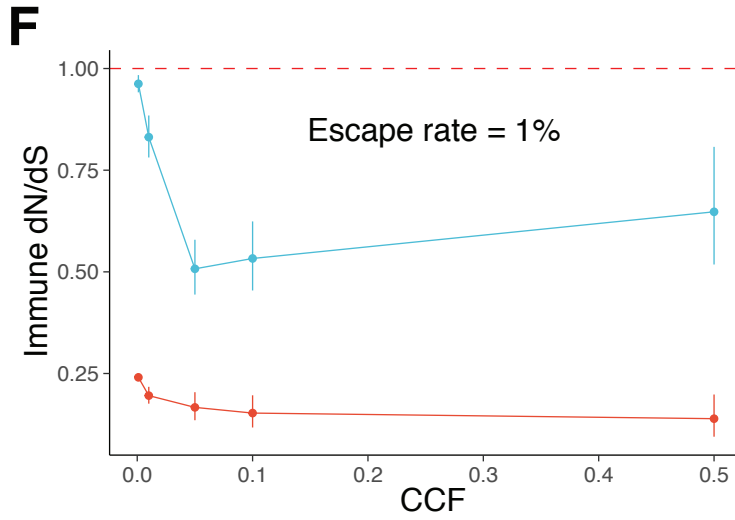
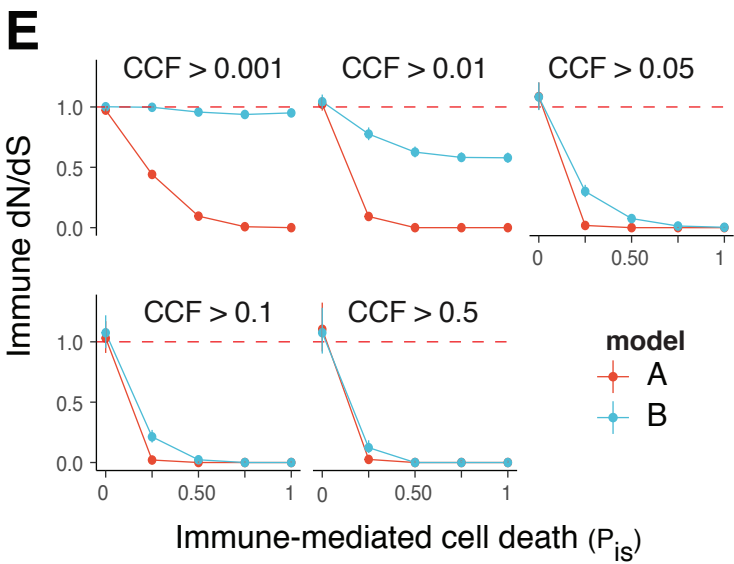
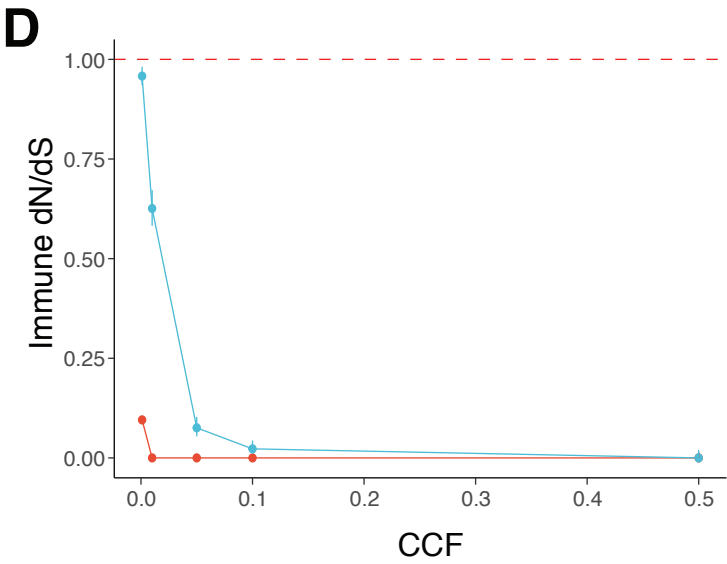
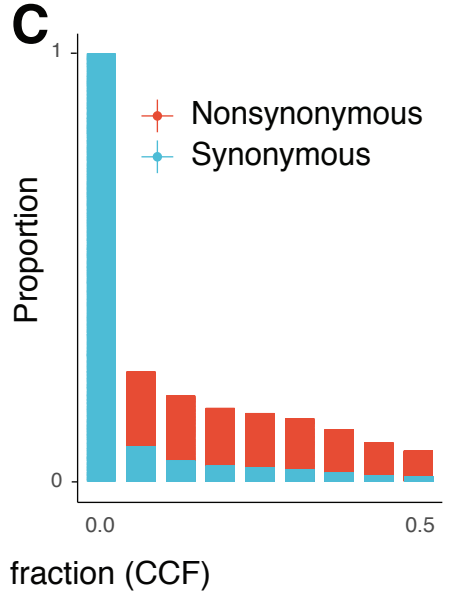
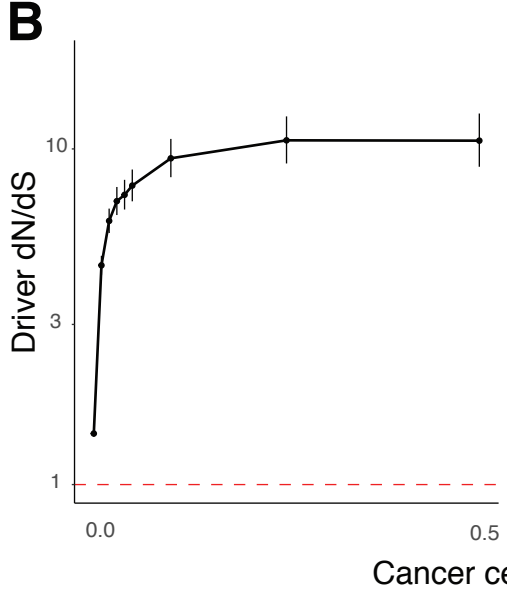
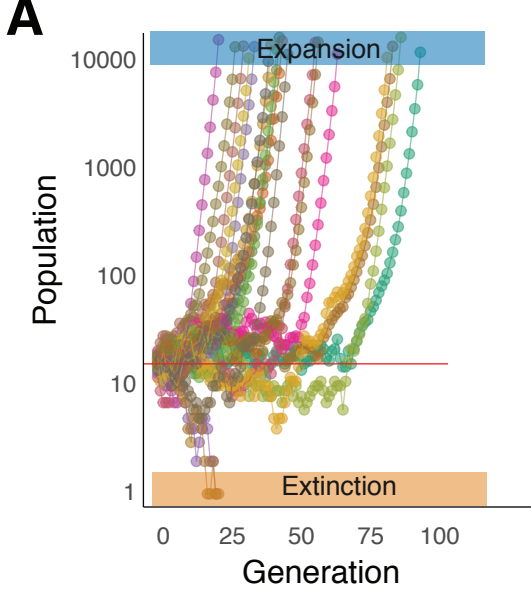
1039 We ran SSB192 (github.com/luisgls/SSB-dNdS) with default parameters to
1040 determine gene and global dN/dS values and SOPRANO
1041 (github.com/luisgls/SOPRANO) using the bed file provided in the package for
1042 HLA-A0201 using 192-base pair correction. We calculated dN/dS for driver genes
1043 using the list of 196 genes provided in Martincorena et al⁷. We calculated SSB-
1044 dNdS and immune dN/dS in the four group categories. For the TCGA patient
1045 specific SOPRANO analysis we used the 4-digit code HLA type for each gene
1046 (HLA-A, HLA-B, and HLA-C). We concatenated all regions predicted to bind to
1047 netMHCpan4.0 as strong binders in those genes that have a median expression
1048 of more than 1FPKM calculated across the 33 TCGA cancer types.

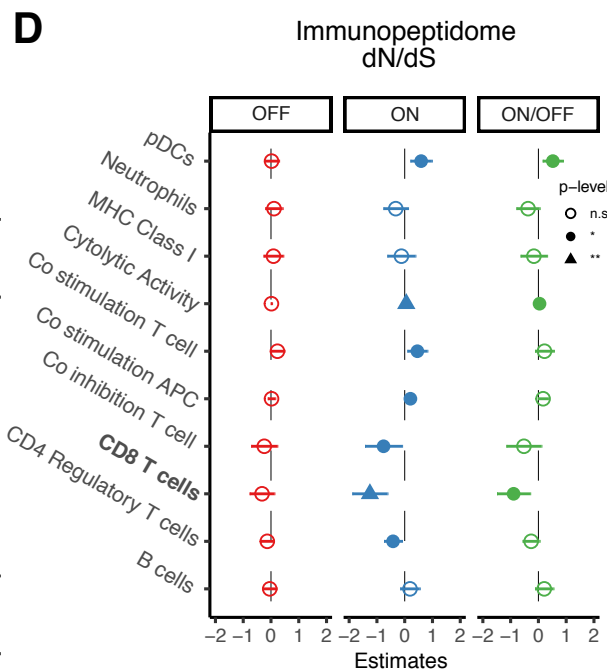
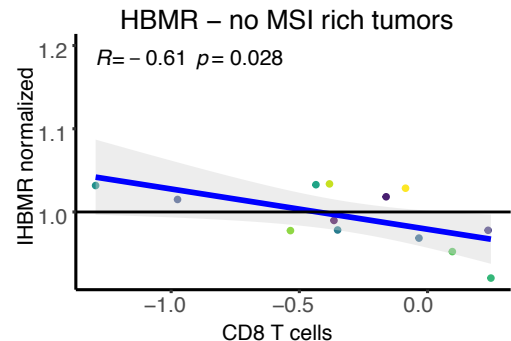
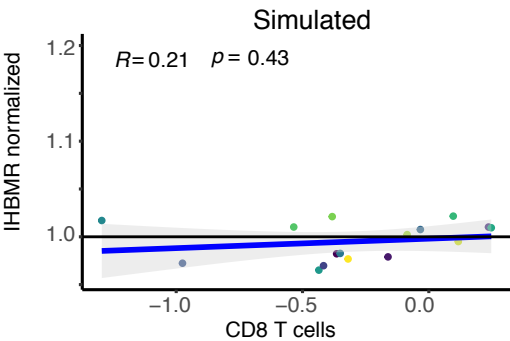
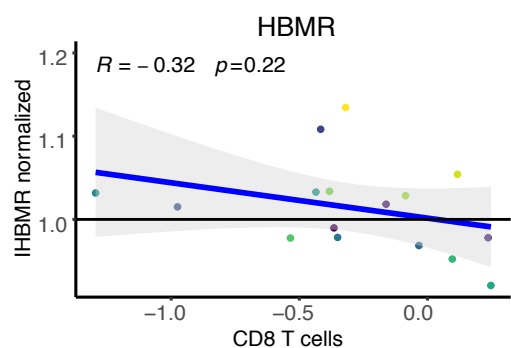
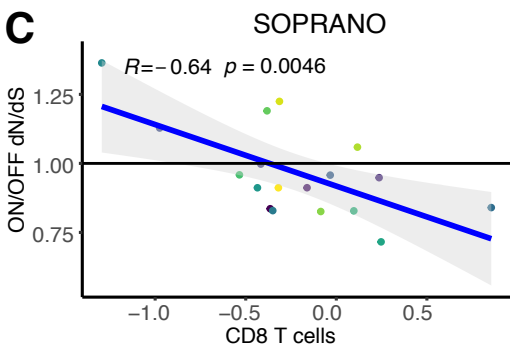
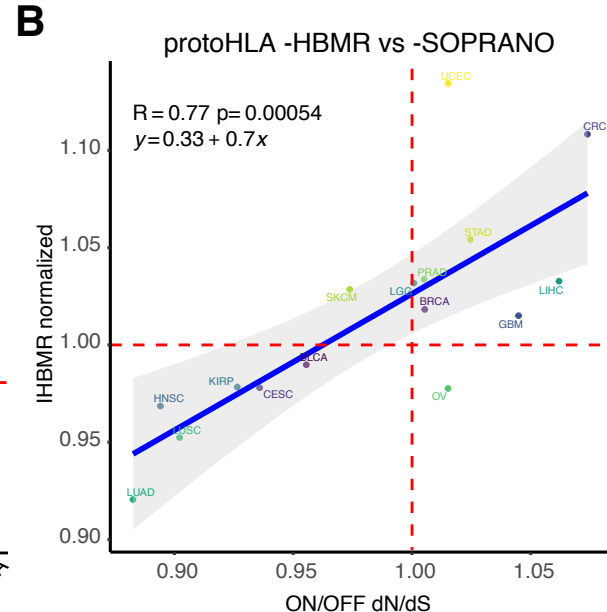
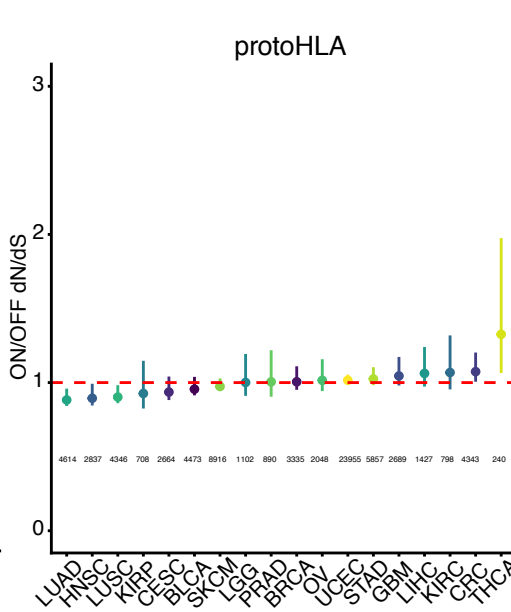
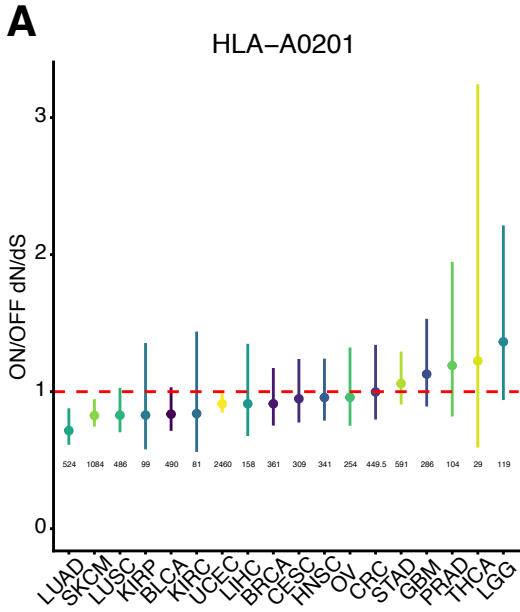


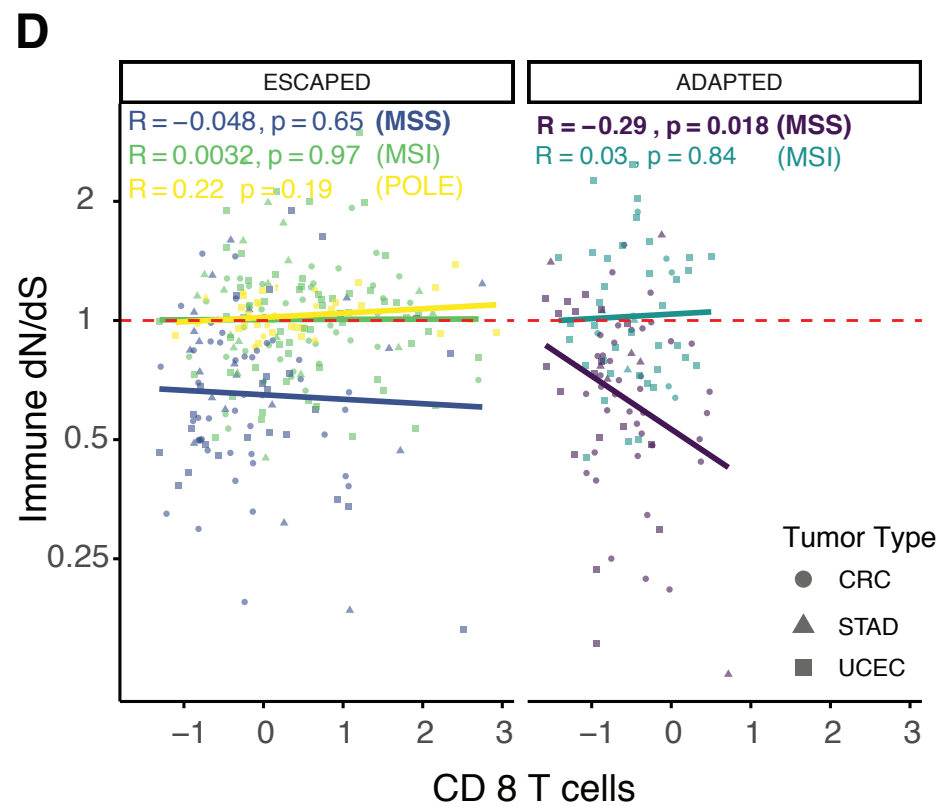
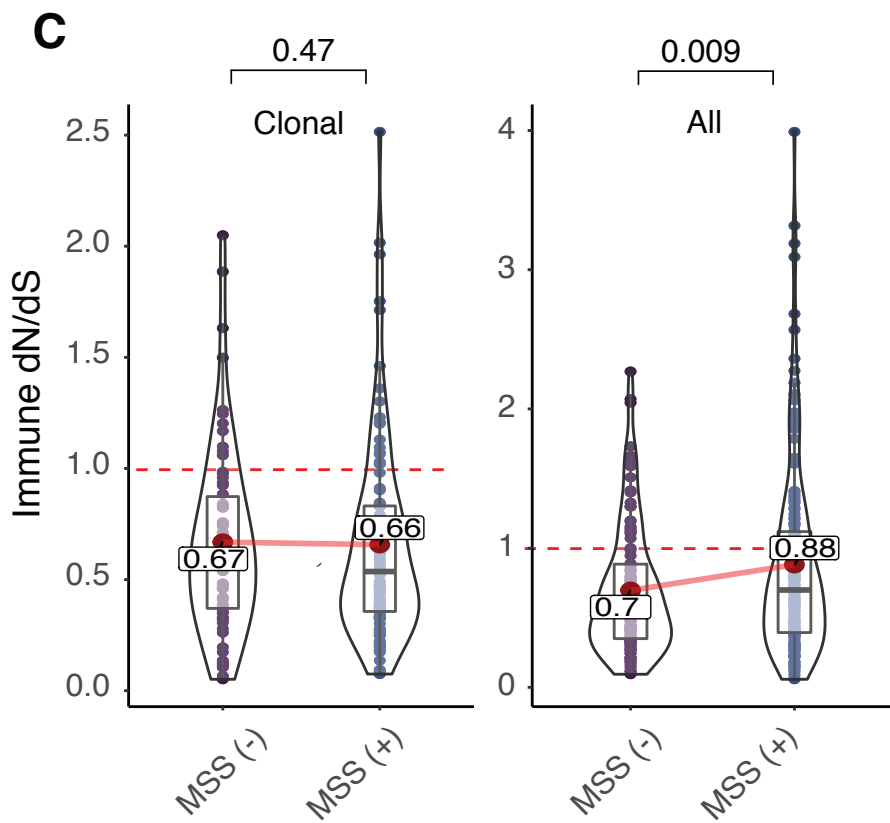
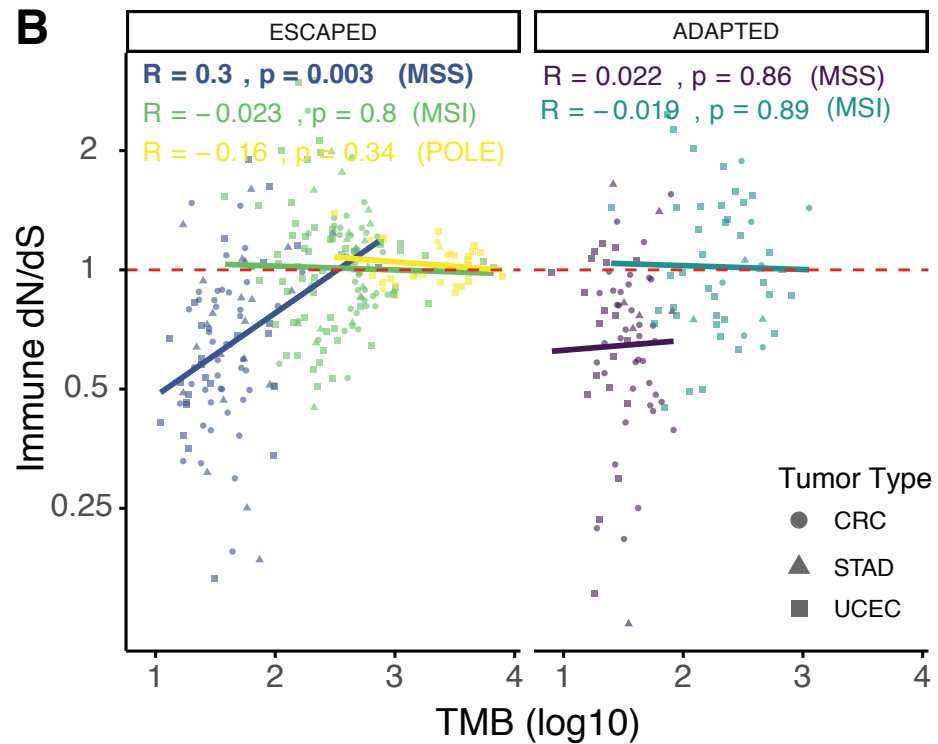
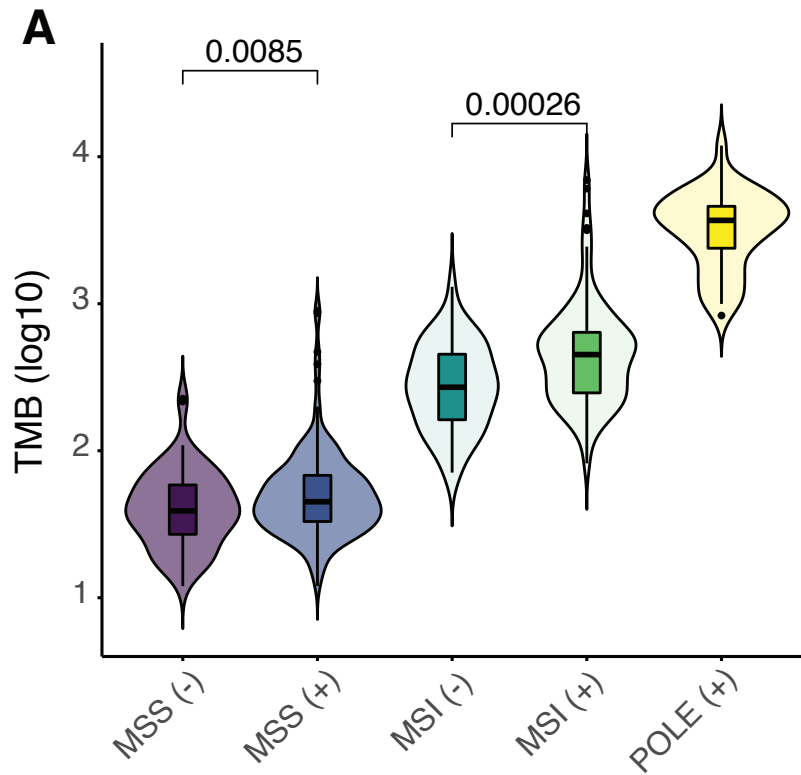
E

Mutations	Proportion
Passenger	~85%- 90%
Driver	0.1%- 1%
Immunogenic	1%- 10%
Escape	0.05%- 5%



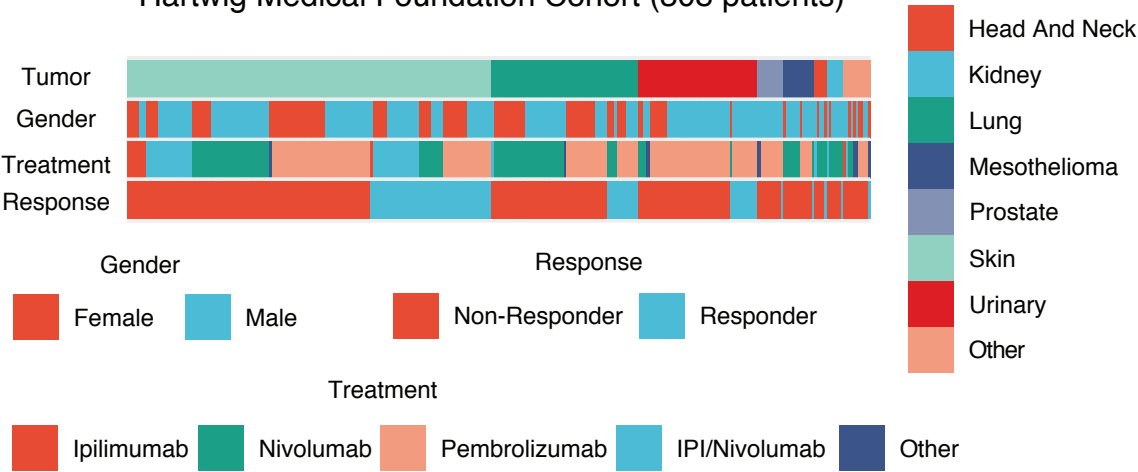




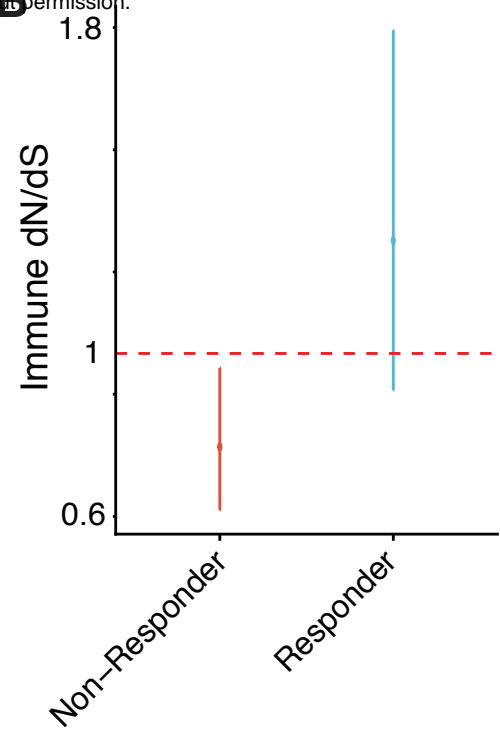


A

Hartwig Medical Foundation Cohort (308 patients)

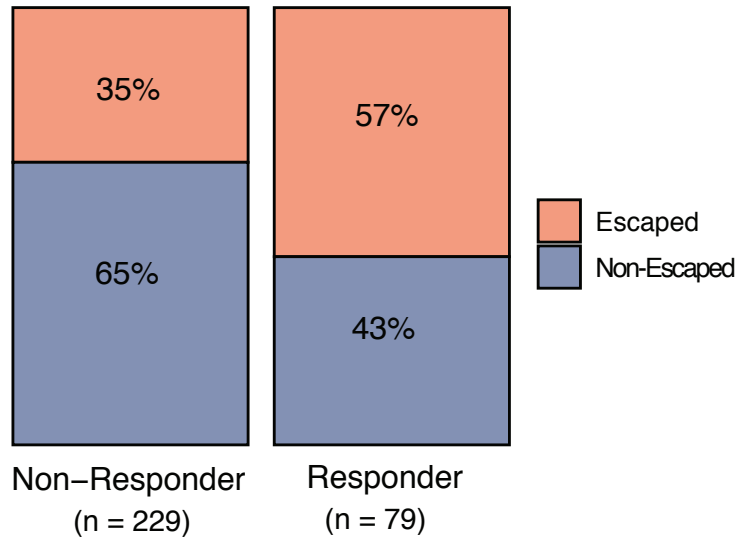


B

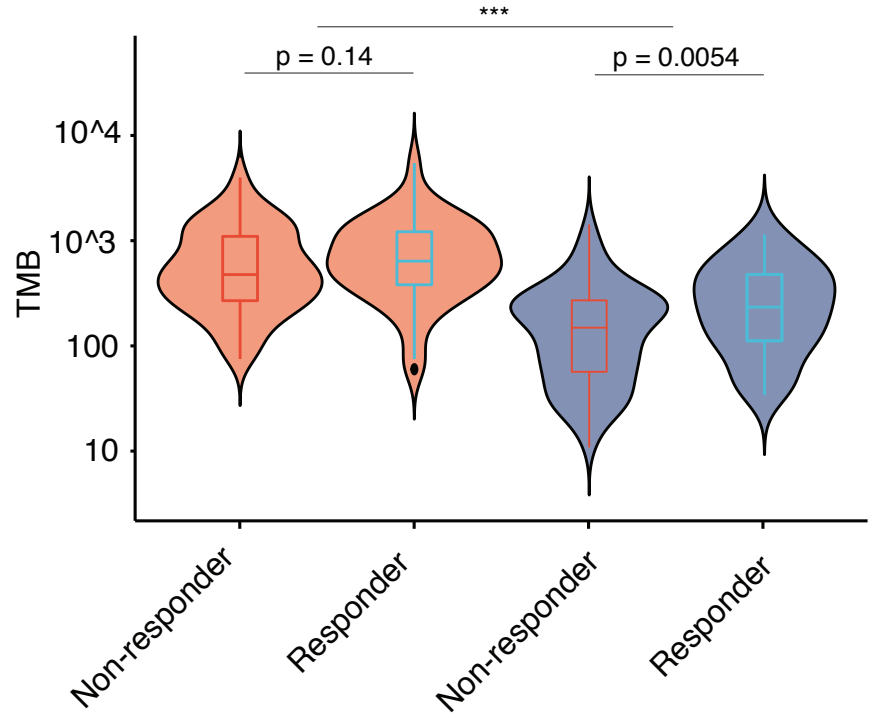


C

$\chi^2 p = 0.001$



D



E

